Department of AERONAUTICS and ASTRONAUTICS
STANFORD UNIVERSITY

PHILIP JHIN

CONTROL OF A SPINNING DRAG-FREE SATELLITE TO REDUCE TRAJECTORY ERRORS DUE TO MASS ATTRACTION

AUGUST
1970

This work was performed in association with research sponsored by the National Aeronautics and Space Administration under Research Grant NsG-~~133~~ NGL-05-020-007

SUDAAR
NO. 408

Department of Aeronautics and Astronautics
Stanford University
Stanford, California

CONTROL OF A SPINNING DRAG-FREE SATELLITE TO REDUCE TRAJECTORY ERRORS DUE TO MASS ATTRACTION

by

Philip Jhin

SUDAAR NO. 408

August 1970

This work was performed in association with research sponsored by the National Aeronautics and Space Administration under Research Grant ~~NsG 133~~ NGL-05-020-007

ABSTRACT

In a drag-free satellite, a proof mass is enclosed in the cavity of a spinning satellite. Control jets on the satellite keep the proof mass from touching the cavity wall. Mass attraction of the satellite on the proof mass is the largest force perturbing the proof mass from a purely planetary gravitational orbit.

This thesis analyzes an integral controller designed to reduce in-track trajectory error caused by mass attraction. Root locus obtained by the frequency symmetry method was used along with analog and digital computer simulations. Linear and on-off controls with square and octagonal deadspace were compared.

The external disturbance forces on the satellite were studied with respect to the mass attraction force that results.

An error analysis was made of the integral controller mechanization. It was shown that the in-track trajectory error caused by mass attraction is reduced from 150 km to 72 m (after 1 year) with the use of integral control.

Trapping, a stable equilibrium position of the proof mass which requires a constant expenditure of fuel, was encountered during the analysis of the integral control. An analysis is made of the trapping susceptibility of a system versus the control gain.

CONTENTS

CONTENTS (Cont)

LIST OF ILLUSTRATIONS

LIST OF SYMBOLS

a_j	Fourier coefficients in expansion of x_{bi}, y_{bi}
A_s	Satellite reference area
c	$\cos(\omega_h t)$
c_D	Satellite drag coefficient
$\bar{c}$	mechanized value of $\cos(\omega_h t)$
c_2	$\cos(2\omega_h t)$
C	$1/2(\partial f_{ex}/\partial x + \partial f_{ey}/\partial y)$
C_r	$1/2(\partial f_{ex}/\partial y + \partial f_{ey}/\partial x)$
ΔC	$1/2(\partial f_{ex}/\partial x - \partial f_{ey}/\partial y)$
e_x, e_y	Nonlinear control signals
e'_x, e'_y	Control signals
f_{bx}, f_{by}, f_{bz}	Components of body-fixed specific force $\vec{F}_b/m_s$ in x,y,z reference frame
f_{cx}, f_{cy}, f_{cz}	Components of control specific force $\vec{F}_c/m_s$ in x, y,z reference frame
f_{eh}	Component of specific force on the proof mass caused by satellite mass attraction in the local horizontal direction
$\tilde{f}_{eh}$	Long term average value of f_{eh}

f_{ex}, f_{ey}	Components of specific force on the proof mass caused by satellite mass attraction in the x,y,z reference frame
f_{ix}, f_{iy}, f_{iz}	Components of external specific force $\vec{F}_i/m_s$ in x, y,z reference frame
f_m	Magnitude of on-off control force
$\vec{F}_b$	Body fixed force on satellite
$\vec{F}_c$	Control force on satellite
$\vec{F}_i$	External disturbance force on satellite
h	In-track trajectory error
I_{hc}, I_{vc}	Integral of f_{eh}, f_{eh}
K_c	Integral control gain
K_j	ΔCa_j
K_p	Position control gain
m_s	Mass of satellite
r^*	Trapping susceptibility measure number
$\vec{r}_b$	Position vector of proof mass with respect to satellite fixed reference frame
r_c	Radius of satellite cavity
r_d	Deadspace size

$\vec{r}_e$	Position vector of C.M. of satellite with respect to satellite fixed reference frame
s	$\sin(\omega_h t)$
$\bar{s}$	Mechanized value of $\sin(\omega_h t)$
s_2	$\sin(2\omega_h t)$
$S_{1,2,3}$	Poles of integral controlled system
S	Laplace transform variable
t	Time
u_b, v_b	dx_b/dx, dy_b/dt
ΔV	Impulse size of on-off controller
V_o	Orbital velocity of satellite
$\dot{W}$	Rate of fuel expenditure
x_b, y_b, z_b	Components of $\vec{r}_b$ in satellite fixed reference frame
x_{bi}, y_{bi}	Components of $\vec{r}_b$ in a locally level reference frame
$x_{b_{ss}}, y_{b_{ss}}$	Steady state value of x_b, y_b
x_e, y_e	Components of $\vec{r}_e$ in satellite fixed reference frame
x_u, y_u	Position bias in integral controller
z	$x_b + iy_b$

β	Dimensionless control parameter
γ	Ratio of velocity gain to position gain
δ	Dimensionless control parameter
ϵ	Deviation of limit cycle frequency from resonant frequency
η	Dimensionless control parameter
θ	Angle for transformation of x_b, y_b to polar coordinates
ρ	Atmospheric density
ω_h	Spin rate with respect to local horizontal
$\bar{\omega}_h$	Mechanized value of ω_h
ω_{lc}	Limit cycle frequency
ω_o	Orbital rate
ω_s	Spin rate
$\vec{\omega}_s$	Satellite angular velocity vector
μ	Earth's gravitational constant

ACKNOWLEDGMENTS

The author is indebted to his advisor, Dr. Daniel B. DeBra, who made it possible for him to apply his classroom knowledge for the first time, to do very interesting research, and at the same time complete his degree requirement. He is also very grateful to both Dr. DeBra and Dr. J. David Powell, who spent many hours with him in very helpful discussions and offered many constructive criticisms. Support for computation under National Aeronautics and Space Administration Research Grant NsG 133 is also gratefully acknowledged.

Chapter I

INTRODUCTION

A. Problem Statement

The drag-free satellite studied in this thesis consists of a proof mass inside a sealed cavity of a spinning satellite. Control jets enable the satellite to follow the trajectory of the proof mass and yet never touch it. In this manner, the proof mass (and therefore the satellite) is made to follow an orbit which is almost solely under the influence of planetary gravity.

Mass attraction force of the satellite on the proof mass is the largest force perturbing this orbit; and for some drag-free satellite applications, this perturbation cannot be tolerated.

Since the satellite will be spinning, mass attraction force at the control sensor null point will not produce long term trajectory error. However, due to the inability to precisely locate every mass element in the satellite, mass attraction gradients will not be zero. This implies that forces which disturb the satellite and displace the proof mass relative to the satellite may result in mass attraction force on the proof mass. This force, due to the gradient in the mass attraction field of the satellite, will systematically act in the direction of the disturbance. Hence it is not averaged by the spin and can have a significant effect on the orbit.

B. Previous Results

In 1964, Lange [2] studied the linear control of translational motions of a spinning vehicle, and he also studied the external disturbance forces on a satellite.

In 1970, Powell [1] designed an on-off translational controller with deadspace for a spinning satellite. He observed the trapping phenomenon and developed a digital program to find trapped solutions and determine the trapping susceptibility of a system.

C. New Results

The main purpose of this thesis is to study the integral controller which has been proposed to reduce in-track trajectory errors caused by mass attraction force.

To this end, the thesis contributes the following results:

(1) Disturbance forces on the satellite and their resulting mass attraction forces on the proof mass were calculated.

(2) The integral controller (linear and with deadspace) stability was analyzed through the use of frequency symmetry, root locus method.

(3) The use of the integral controller was shown to reduce in-track trajectory error caused by mass attraction from 150 km to 72 m (after 1 year).

(4) Limit cycle behavior of the proof mass, at the frequencies determined by practical impulse sizes ($5 \times 10^{-3} > \Delta V > 5 \times 10^{-4}$ mm/sec), was shown to cause no significant in-track trajectory error due to mass attraction.

(5) Trapping susceptibility (trapping is a stable equilibrium position of the proof mass which requires constant fuel expenditure) was shown to be almost constant for $K_p/\omega_s^2 > 1$, the range of K_p/ω_s^2 which will be used in practice. For $K_p/\omega_s^2 < 1$, it was shown that this susceptibility reduces very rapidly.

Chapter II

DESCRIPTION OF SATELLITE WITH LINEAR NON-INTEGRAL CONTROL

The basic drag-free satellite structure is described. Equations of motion for the spinning satellite is given, and a linear non-integral controller is described.

A. Satellite Description

The drag-free satellite (Fig. 1) consists of a proof mass enclosed in the sealed cavity of a spinning satellite. The satellite has control jets which keep the proof mass away from the cavity wall. The proof mass is therefore free from the external disturbing forces such as atmospheric drag, solar radiation, etc., and the largest force that perturbs the proof mass from a purely planetary gravitational orbit is mass attraction between the satellite and the proof mass.

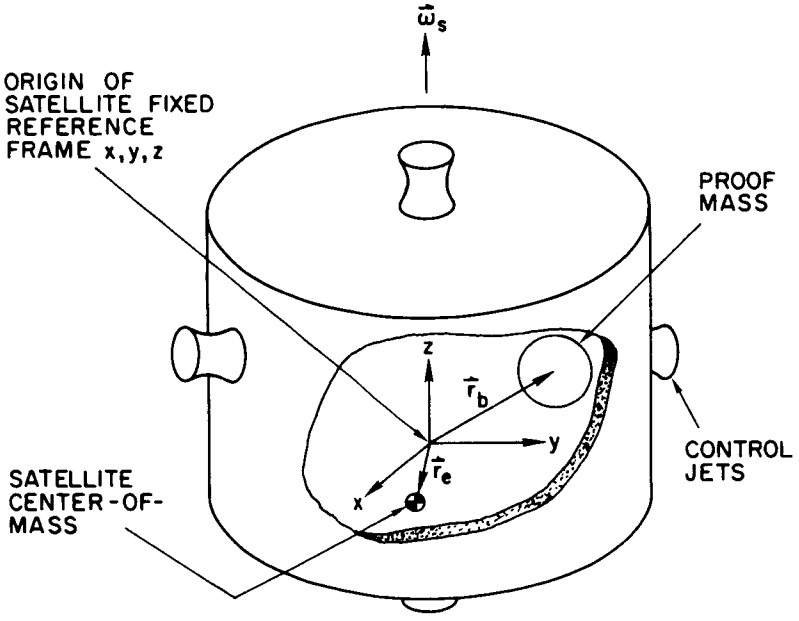

Fig. 1. DRAG-FREE SATELLITE SCHEMATIC.

The satellite contains a sensor (capacitive or optical) which measures the proof mass position relative to the satellite. Using this information, the relative proof mass velocity is estimated (this is discussed in detail by Powell [1]). The position and velocity information are then fed into the controller to generate a command for a control force.

B. Equations of Motion

Assume that the satellite center-of-mass position is constant and that $\dot{\vec{\omega}}_s = 0$. Neglect gravitational forces on the satellite and all forces on the proof mass (mass attraction force on the proof mass will be studied as a correction to these equations). With these assumptions, the equations of motion are given by Powell in Reference 1 as,

$$\ddot{\vec{r}}_b + 2\vec{\omega}_s \times \dot{\vec{r}}_b + \vec{\omega}_s \times (\vec{\omega}_s \times \vec{r}_b) = \frac{1}{m_s} (\vec{F}_i + \vec{F}_b + \vec{F}_c) + \vec{\omega}_s \times (\vec{\omega}_s \times \vec{r}_e) \tag{2.1}$$

where

$\vec{F}_b$ = disturbing forces fixed to the rotating satellite

$\vec{F}_c$ = control force on the satellite

$\vec{F}_i$ = all other nongravitational perturbing forces on the satellite

$\vec{\omega}_s$ = satellite spin rate

m_s = mass of satellite

$\vec{r}_b, \vec{r}_e$ are as defined in Fig. 1.

With the choice of reference frame as shown in Fig. 1, the equations of motion becomes,

$$\ddot{x}_b - \omega_s^2 x_b - 2\omega_s \dot{y}_b = f_{ix} + f_{bx} + f_{cx} - \omega_s^2 x_e \tag{2.2a}$$

$$\ddot{y}_b - \omega_s^2 y_b + 2\omega_s \dot{x}_b = f_{iy} + f_{by} + f_{cy} - \omega_s^2 y_e \tag{2.2b}$$

$$\ddot{z}_b = f_{iz} + f_{bz} + f_{cz} \tag{2.2c}$$

The z-axis $1/(s^2)$ plant, uncoupled from the other two equations, is well understood and will henceforth be disregarded.

C. Linear Non-Integral Control

The linear control law used by Powell [1] is,

$$f_{cx} = -K_p [x_b + \gamma(\dot{x}_b - \omega_s y_b)] \tag{2.3a}$$

$$f_{cy} = -K_p [y_b + \gamma(\dot{y}_b + \omega_s x_b)] \tag{2.3b}$$

where

$K_p \triangleq$ position gain $(1/\text{sec}^2)$

$\gamma \triangleq \dfrac{\text{velocity gain}}{\text{position gain}}$ (sec)

Substituting the control forces into Eqs. (2.2a) and (2.2b) gives,

$$\begin{bmatrix} \dot{x}_b \\ \dot{y}_b \\ \dot{u}_b \\ \dot{v}_b \end{bmatrix} = \begin{bmatrix} 0 & 0 & 1 & 0 \\ 0 & 0 & 0 & 1 \\ \omega_s^2 - k_p & \gamma\omega_s K_p & -\gamma K_p & 2\omega_s \\ -\gamma\omega_s K_p & \omega_s^2 - K_p & -2\omega_s & -\gamma K_p \end{bmatrix} \begin{bmatrix} x_b \\ y_b \\ u_b \\ v_b \end{bmatrix} + \begin{bmatrix} 0 \\ 0 \\ f_{ix} + f_{bx} - \omega_s^2 x_e \\ f_{iy} + f_{by} - \omega_s^2 y_e \end{bmatrix} \tag{2.4}$$

Chapter III

DISTURBING FORCES

The only significant disturbing force on the proof mass, mass attraction force, is given in a Taylor series expansion. Disturbance forces acting on the satellite which are constant in the satellite fixed reference frame are shown to cause no non-zero average mass attraction force. An order of magnitude is calculated for the largest disturbing force on the satellite which does cause a non-zero average mass attraction force.

A. Mass Attraction Force on the Proof Mass

1. Mass Attraction Force Model

In the reference frame fixed to the satellite (Fig. 1), the specific force on the proof mass caused by mass attraction of the satellite can be represented by a Taylor series expanded about the origin,

$$f_{ex} = f_{ex_o} + \frac{\partial f_{ex}}{\partial x} x_b + \frac{\partial f_{ex}}{\partial y} y_b + \frac{1}{2} \frac{\partial^2 f_{ex}}{\partial x^2} x_b^2 + \frac{1}{2} \frac{\partial^2 f_{ex}}{\partial x \partial y} x_b y_b + \frac{1}{2} \frac{\partial^2 f_{ex}}{\partial y^2} y_b^2 + \frac{1}{6} \frac{\partial^3 f_{ex}}{\partial x^3} x_b^3 + \frac{1}{6} \frac{\partial^3 f_{ex}}{\partial x^2 \partial y} x_b^2 y_b + \frac{1}{6} \frac{\partial^3 f_{ex}}{\partial x \partial y^2} x_b y_b^2 + \frac{1}{6} \frac{\partial^3 f_{ex}}{\partial y^3} y_b^3 + \ldots \tag{3.1a}$$

$$f_{ey} = f_{ey_o} + \frac{\partial f_{ey}}{\partial x} x_b + \frac{\partial f_{ey}}{\partial y} y_b + \frac{1}{2} \frac{\partial^2 f_{ey}}{\partial x^2} x_b^2 + \ldots \tag{3.1b}$$

where f_{ex_o}, f_{ey_o}, $\partial f_{ex}/\partial x$, ... are all evaluated at the origin.

For error analysis, Powell [1] showed that significant trajectory error is caused only by a non-zero average in-track force*, $\tilde{f}_{eh}$ (in-track direction is defined in Fig. 2.),

$$\tilde{f}_{eh} = \frac{1}{T}\int_{T_o}^{T_o+T} f_{eh}\, dt \qquad T \approx 1 \text{ day} \qquad (3.2a)$$

$$f_{eh} = c\, f_{ex} - s f_{ey} \qquad (3.2b)$$

where

$c \triangleq \cos(\omega_h t)$

$s \triangleq \sin(\omega_h t)$

$\omega_h \triangleq \omega_s - \omega_o$

$\omega_o \triangleq$ orbital rate $\simeq 10^{-3}$ rad/sec

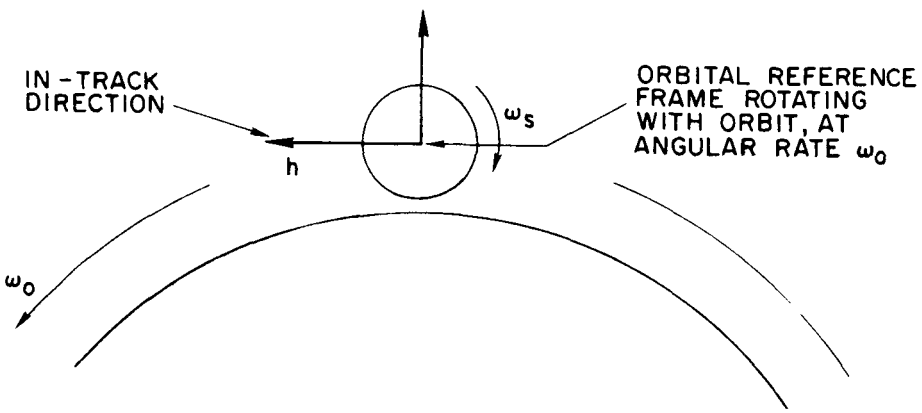

Fig. 2. ORBITAL REFERENCE FRAME.

Combining Eqs. (3.1a,b) and Eq. (3.2b), we see that f_{ex_o} and f_{ey_o} are modulated by cos $(\omega_h t)$ and sin $(\omega_h t)$ respectively. ω_h will be chosen such that $2\pi/\omega_h \ll 1$ day, so f_{ex_o} and f_{ey_o} do not contribute to $\tilde{f}_{eh}$. Due to the inability to precisely locate each mass element, there will be non-zero gradients,

*This conclusion is arrived at by a frequency domain analysis of the in-track trajectory error equation, Eq. (5.2).

where $\frac{\partial f_{ex,y}}{\partial x}$, $\frac{\partial f_{ex,y}}{\partial y} \simeq 10^{-10}$ g/mm ,

and Fleming [3] has shown that

$$\frac{\partial^{n+1} f_{ex,y}}{\partial x^{n+1}} \simeq \frac{1}{10} \frac{\partial^{n} f_{ex,y}}{\partial x^{n}} \quad .$$

2. Mass Attraction Force Due to Body-Fixed Disturbance Forces on, or Center of Mass Offset of the Satellite

A force on the satellite which is constant in the satellite fixed reference frame (Fig. 1), results in constant "steady-state" errors in x_b and y_b (Fig. 3). This force can be due either to an externally applied force or a center of mass offset (non-zero x_e and/or y_e).

Setting $x_b = y_b = u_b = v_b = 0$ in Eq. (2.4), we get the "steady state" errors $x_{b_{ss}}$ and $y_{b_{ss}}$,

$$\begin{bmatrix} x_{b_{ss}} \\ y_{b_{ss}} \end{bmatrix} = \begin{bmatrix} \omega_s^2 - K_p & \gamma\omega_s K_p \\ -\gamma\omega_s K_p & \omega_s^2 - K_p \end{bmatrix}^{-1} \begin{bmatrix} \omega_s^2 x_e - f_{bx} \\ \omega_s^2 y_e - f_{by} \end{bmatrix} \tag{3.3a}$$

or

$$\begin{bmatrix} x_{b_{ss}} \\ y_{b_{ss}} \end{bmatrix} = \frac{\begin{bmatrix} \omega_s^2 - K_p & -\gamma\omega_s K_p \\ \gamma\omega_s K_p & \omega_s^2 - K_p \end{bmatrix}}{\left[\left(\omega_s^2 - K_p\right)^2 + \gamma^2 \omega_s^2 K_p^2\right]} \begin{bmatrix} \omega_s^2 x_e - f_{bx} \\ \omega_s^2 y_e - f_{by} \end{bmatrix} \tag{3.3b}$$

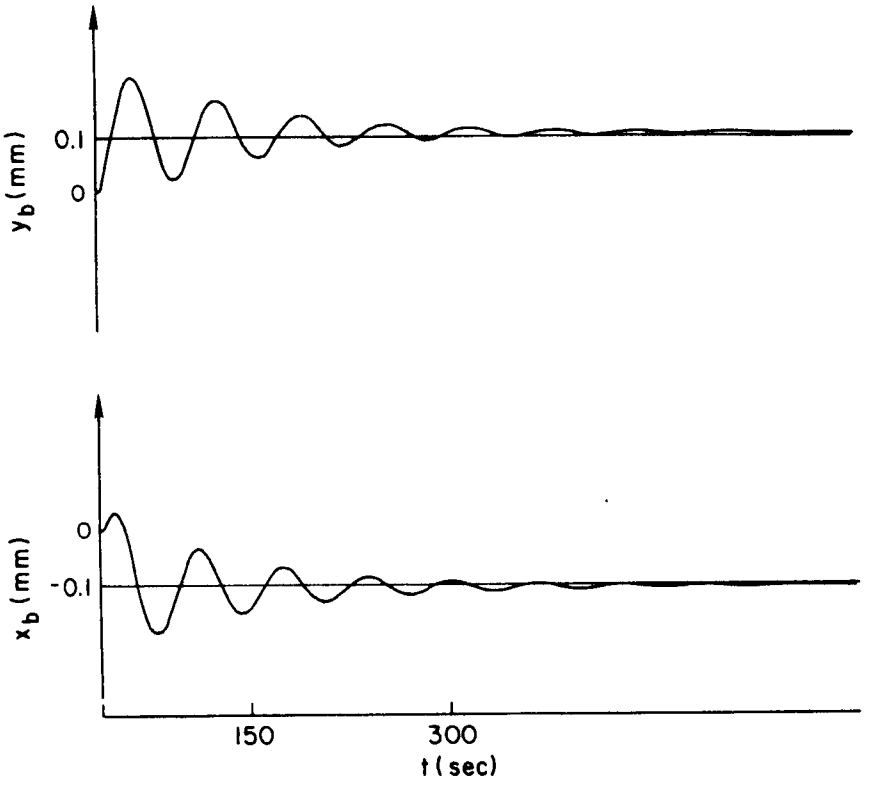

Fig. 3. ANALOG SIMULATION OF EQ. (2.4) TO SHOW EFFECT OF BODY-FIXED FORCES.

with

$$f_{ix} = f_{iy} = 0$$

$$f_{bx} = f_{by} = 10^{-2} \text{ mm/sec}^2$$

$$x_e = y_e = 0$$

$$K_p = 10^{-2} \text{ 1/sec}^2$$

$$\omega_s = 0.1 \text{ rad/sec}$$

$$\gamma = 100 \text{ sec}$$

From Eq. (3.3b),

$$\begin{bmatrix} x_{b_{ss}} \\ y_{b_{ss}} \end{bmatrix} = \begin{bmatrix} 0.1 \\ 0.1 \end{bmatrix} \text{ mm}$$

With constant $x_{b_{ss}}$ and $y_{b_{ss}}$, Eq. (3.2b) becomes

$$f_{eh} = c \times \text{constant} - s \times \text{constant} \tag{3.4}$$

and Eq. (3.2a) becomes,

$$\tilde{f}_{eh} = \frac{1}{\omega_s T} \left\{ s \times \text{constant} + c \times \text{constant} \right\} \Bigg|_{t=T_o}^{t=T_o+T} \tag{3.5}$$

with $T = 1$ day $\tilde{f}_{eh} \cong 0$. Therefore, satellite fixed forces and center of mass offsets will not contribute long term in-track trajectory errors.

3. Mass Attraction Force Due to Other Disturbance Forces on the Satellite

Lange [2] showed that the only significant perturbing force, which is not constant in the satellite fixed frame, is constant atmospheric drag.

Atmospheric drag is constant in the orbital reference frame (Fig. 2), and this suggests sinusoidal "steady-state" errors in x_b and y_b (Fig. 4). Since

$$f_{ix} = \frac{|F_i|}{m_s} \cos(\omega_s t) \tag{3.6a}$$

$$f_{iy} = -\frac{|F_i|}{m_s} \sin(\omega_s t) \tag{3.6b}$$

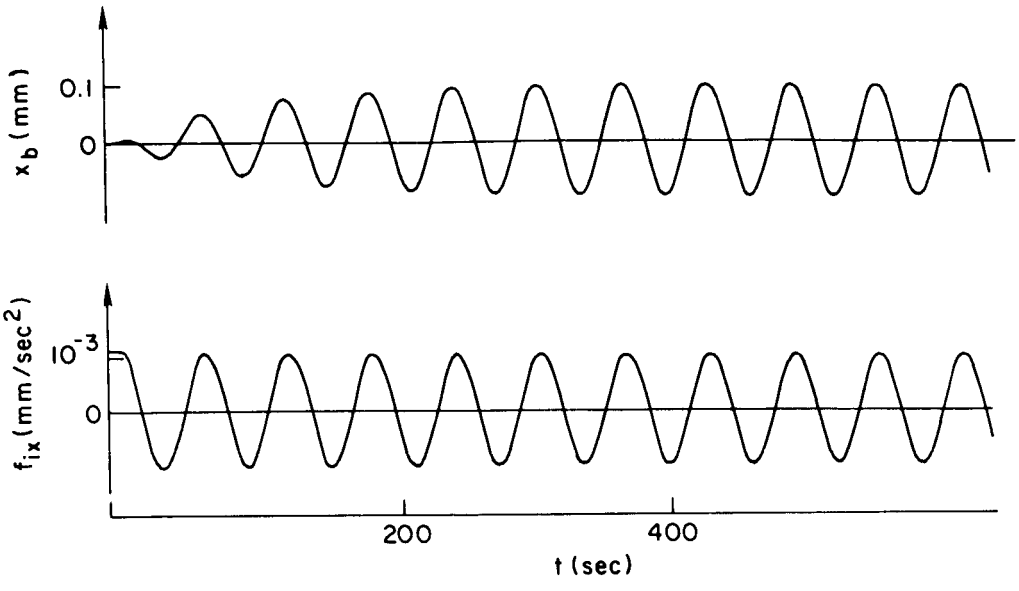

Fig. 4. ANALOG SIMULATION OF EQ. (2.4) TO SHOW SYNCHRONOUS EFFECT OF ATMOSPHERIC DRAG IN BODY AXES, WITH

$$f_{ix} = 10^{-3} \cos(\omega_s t) \text{ mm/sec}^2$$

$$f_{iy} = -10^{-3} \sin(\omega_s t) \text{ mm/sec}^2$$

$$f_{bx} = f_{by} = 0$$

$$x_e = y_e = 0$$

$$K_p = 10^{-3} \text{ 1/sec}^2$$

$$\omega_s = 0.1 \text{ rad/sec}$$

$$\gamma = 100 \text{ sec}$$

where $|F_i|$ = magnitude of the disturbance force. We get from Eq. (2.4),

$$x_{b_{ss}} = \frac{|F_i|}{m_s K_p} \cos(\omega_s t) = \frac{f_{ix}}{K_p} \tag{3.7a}$$

$$x_{b_{ss}} = \frac{|F_i|}{m_s K_p} \sin(\omega_s t) = \frac{f_{iy}}{K_p} \tag{3.7b}$$

Combining Eqs. (3.7a,b) and Eq. (3.2b),

$$f_{eh} = cf_{ex_o} - sf_{ey_o} + \frac{|F_i|}{m_s K_p}\left[cs\left(\frac{\partial f_{ex}}{\partial x} - \frac{\partial f_{ex}}{\partial y}\right)\right.$$

$$\left. + c^2\left(\frac{\partial f_{ex}}{\partial x}\right) + s^2\left(\frac{\partial f_{ey}}{\partial x}\right)\right] + \text{terms containing } (s^i c^j)$$

$$\text{where } i + j > 2\ , \tag{3.8}$$

and

$$\tilde{f}_{eh} = \frac{1}{\omega_s T}\left\{sf_{ex_o} + cf_{ey_o} + \frac{|F_i|}{2m_s K_p}\left[s^2\left(\frac{\partial f_{ex}}{\partial x} - \frac{\partial f_{ey}}{\partial y}\right)\right.\right.$$

$$\left.\left. + \left(\frac{1}{2}cs + .05t\right)\left(\frac{\partial f_{ex}}{\partial y} - \frac{\partial f_{ey}}{\partial x}\right)\right] + \text{terms containing}\right.$$

$$\left.(s^i c^j) \text{ where } i + j > 1\right\}_{t=T_o}^{t=T_o+T}$$

$$\tilde{f}_{eh} \neq 0 \quad \text{for } T \geq 1 \text{ day.} \tag{3.9}$$

Therefore, atmospheric drag will cause long term in-track trajectory error.

B. Atmospheric Drag Force on the Satellite

In order to study the control to reduce trajectory errors, we need to know the magnitude of the atmospheric drag.

$$F_{Drag} = \frac{1}{2} \rho V_o^2 c_D A_s \qquad (3.10)$$

where

ρ = atmospheric density

V_o = orbit speed

c_D = drag coefficient

A_s = satellite reference area.

Considering a typical satellite with,

$$c_D = 2$$

$$A_s = 3 \times 10^5 \text{ mm}^2$$

$$m_s = 90 \text{ kg}$$

$$H = 400 \text{ km}$$

$$\rho = 6.5 \times 10^{-18} \text{ gm/mm}^3$$

and

$$V_o = \sqrt{\frac{\mu}{R_E + H}} = 0.77 \times 10^7 \text{ mm/sec}$$

where

$\mu = GM = 3.98 \times 10^{23} \text{ mm}^3/\text{sec}^2$

R_E = radius of earth = 6.38×10^9 mm

$$f_{Drag} = \frac{F_{Drag}}{m_s} = 1.24 \times 10^{-3} \text{ mm/sec}^2$$

C. Conclusion

Because of inability to pinpoint every mass element of the satellite, there will be mass attraction force gradients. These gradients, combined

with a constant atmospheric drag force of 10^{-3} mm/sec^2 (10^{-7}g), will result in long term in-track trajectory errors of 150 km per year.

Chapter IV

INTEGRAL CONTROLLER WITH SQUARE DEADSPACE

Integral controller with square deadspace is described. It is analyzed both by use of the root locus method and computer simulations. Since in actual design, the satellite will have both an on-off controller and on octagonal or circular deadspace, both these features are added on and simulated on computer. This is to show that the basic analysis done on the simpler square deadspace system is still valid.

A. Description of Integral Control with Square Deadspace

Powell [1] suggested an integral controller to reduce the trajectory error caused by mass attraction. A square deadspace is incorporated in the controller to reduce sensitivity to chatter about the sensor null point and to noise when an on-off controller is used.

1. Control Equations

In order to reduce errors caused by mass attraction force, we must limit the integral given by Eq. (3.2a).

We can do this by introducing a control center bias,

$$\begin{bmatrix} x_u \\ y_u \end{bmatrix} = -K_c \begin{bmatrix} c & -s \\ s & c \end{bmatrix}^{-1} \begin{bmatrix} I_{hc} \\ I_{vc} \end{bmatrix} \tag{4.1}$$

where

$$\begin{bmatrix} I_{hc} \\ I_{vc} \end{bmatrix} = \int_0^t \begin{bmatrix} x_{bi} \\ y_{bi} \end{bmatrix} dt \tag{4.2}$$

and

$$\begin{bmatrix} x_{bi} \\ y_{bi} \end{bmatrix} = \begin{bmatrix} c & -s \\ s & c \end{bmatrix} \begin{bmatrix} x_b \\ x_b \end{bmatrix} \tag{4.3a}$$

$K_c \triangleq$ integral control gain

The control law then becomes,

$$f_{cx} = -K_p[x_b - x_u + \gamma(\dot{x}_b - \omega_s y_b)] \tag{4.3b}$$

$$f_{cy} = -K_p[y_b - y_u + \gamma(\dot{y}_b + \omega_s x_b)] \tag{4.3c}$$

2. Square Deadspace

The integral control law with square deadspace becomes,

$$f_{cx} = -K_p e_x \tag{4.4a}$$

$$f_{cy} = -K_p e_y \tag{4.4b}$$

where e'_x, e'_y are related to e_x, e_y by the relationship shown in Fig. 5, and

$$e'_x = x_b - x_u + \gamma(\dot{x}_b - \omega_s y_b) \tag{4.5a}$$

$$e'_y = y_b - y_u + \gamma(\dot{y}_b + \omega_s x_b) \tag{4.5b}$$

B. Effect of Integral Control

To analyze the integral controller, both the root locus method and computer simulations were used.

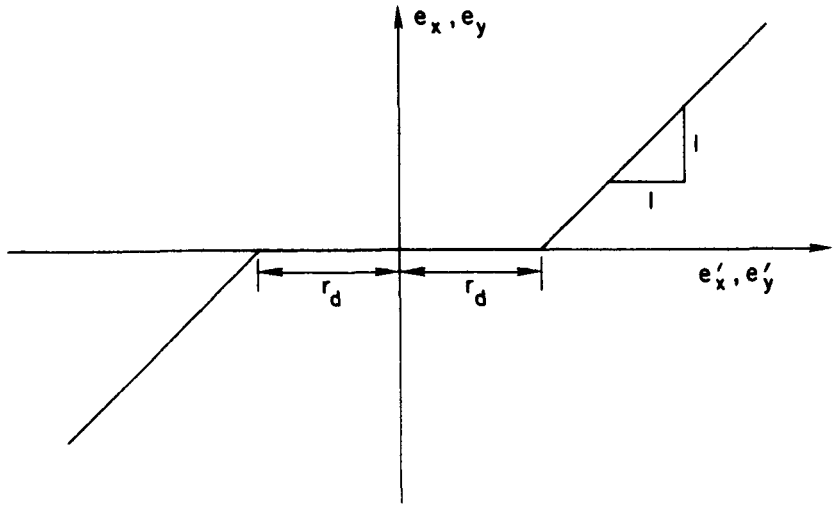

Fig. 5. DEADBAND DEFINITION FOR EACH AXIS FOR SQUARE DEADSPACE.

1. Root Locus Analysis

From Chapter IV-A-1,

$$x_u = -K_c[cI_{hc} + sI_{vc}]$$

$$= -K_c\left\{c\int_0^t [cx_b - sy_b]\,dt + s\int_0^t [sx_b + cy_b]\,dt\right\} \qquad (4.6a)$$

$$y_u = -K_c[-sI_{hc} + cI_{vc}]$$

$$= -K_c\left\{-s\int_0^t [cx_b - sy_b]\,dt + c\int_0^t [sx_b + cy_b]\,dt\right\} \qquad (4.6b)$$

The characteristic equation is obtained by the frequency symmetry method. Substitute Eqs. (4.6a,b) into Eqs. (4.5a,b) respectively,

$$e_x = x_b + K_c \left\{ c \int_0^t [cx_b - sy_b]\, dt + s \int_0^t [sx_b + cy_b]\, dt \right\}$$

$$+ \gamma(\dot{x}_b - \omega_s y_b) \tag{4.7a}$$

$$e_y = y_b + K_c \left\{ -s \int_0^t [cx_b - sy_b]\, dt + c \int_0^t [sx_b + cy_b]\, dt \right\}$$

$$+ \gamma(\dot{y}_b + \omega_s x_b) \tag{4.7b}$$

Substitute Eqs. (4.7a,b) into Eqs. (2.2a,b) respectively, with $f_{bx} = f_{by} = x_e = y_e = 0$,

$$\ddot{x}_b - \omega_s^2 x_b - 2\omega_s \dot{y}_b = f_{ix} - K_p e_x \tag{4.8a}$$

$$\ddot{y}_b - \omega_s^2 y_b + 2\omega_s \dot{x}_b = f_{iy} - K_p e_y \tag{4.8b}$$

Linear control with no deadspace is used here to make it possible to draw a root locus plot. In the next section, it will be shown that these results, obtained without a deadspace, are equally valid for control with deadspace.

Add j times Eq. (4.8b) to Eq. (4.8a) $(j = \sqrt{-1})$,

$$(\ddot{x}_b + j\ddot{y}_b) - \omega_s^2 (x_b + jy_b) + 2j\omega_s (\dot{x}_b + j\dot{y}_b)$$

$$= (f_{ix} + jf_{iy}) - K_p (x_b + jy_b) - K_p K_c \left\{ c \int_0^t [cx_b - sy_b]\, dt \right.$$

$$\left. + s \int_0^t [sx_b + cy_b]\, dt \right\} + j \left\{ -s[cx_b - sy_b]\, dt \right.$$

$$\left. + c \int_0^t [sx_b + cy_b]\, dt \right\} - K_p \gamma [(\dot{x}_b + j\dot{y}_b) + j\omega_s (x_b + jy_b)] \tag{4.9}$$

Let $z \triangleq x_b + jy_b$ in Eq. (4.7)

$$\ddot{z} - \omega_s^2 z + 2j\omega_s \dot{z} = -K_p z - K_p K_c \left\{ c \int_0^t (c + js)\, z dt \right.$$

$$\left. + s \int_0^t (s - jc)\, z dt \right\} - K_p \gamma [\dot{z} + j\omega_s z] \qquad (4.10)$$

Using the trigometric identities,

$$c = \frac{1}{2} \left(e^{j\omega_h t} + e^{-j\omega_h t} \right)$$

and

$$s = \frac{1}{2j} \left(e^{j\omega_h t} - e^{-j\omega_h t} \right)$$

Eq. (4.10) becomes,

$$\ddot{z} + (2j\omega_s + k_p \gamma)\dot{z} - \left(\omega_s^2 - K_p - j\omega_s K_p \gamma \right) z$$

$$+ K_p K_c \left\{ e^{-j\omega_h t} \int_0^t e^{j\omega_h t} z\, dt \right\} = 0 \qquad (4.11)$$

Taking the Laplace transform of Eq. (4.11) and noting that,

$$\mathcal{L}\left\{ \int_0^t e^{j\omega_h t} z dt \right\} = \frac{1}{S} \mathcal{L}\left\{ e^{j\omega_h t} z \right\}$$

$$= \frac{1}{S} Z(S - j\omega_h)$$

and

$$\mathcal{L}\left\{e^{-j\omega_h t}\int_0^t e^{j\omega_h t}\, z\, dt\right\} = \frac{Z(S)}{S + j\omega_h}$$

we get,

$$\left[S^2 + (2j\omega_s + K_p\gamma)S - \left(\omega_s^2 - K_p - j\omega_s K_p\gamma\right) + \frac{K_p K_c}{S + j\omega_h}\right] Z(S) = 0 \qquad (4.12)$$

Writing the characteristic equation in Evans root locus form,

$$\frac{K_c K_p}{(S + j\omega_h)\left[S^2 + (2j\omega_s + K_p\gamma)S - \left(\omega_s^2 - K_p - j\omega_s\gamma K_p\right)\right]} = -1 \qquad (4.13)$$

The pole locations, are

$$S_{1,2} = \frac{-(2j\omega_s + K_p\gamma) \pm \sqrt{(2j\omega_s + K_p\gamma)^2 + 4\left(\omega_s^2 - K_p - j\omega_s\gamma K_p\right)}}{2} \qquad (4.14a)$$

$$S_3 = -j\omega_h \qquad (4.14b)$$

Note that poles $S_{1,2}$ in Fig. 6 are poles of the original system without integral control, and pole S_3 is the integral controller pole.

In general, a root locus plot for the integral controller can be obtained from the root locus plot of the original non-integral control system (Fig. 7). The characteristic equation for the non-integral system in Evans root locus form is,

$$\frac{\frac{K_p}{\omega_s^2}(\gamma\omega_s S' + 1 + j\gamma\omega_s)}{S'^2 + 2jS' - 1} = -1 \qquad (4.15)$$

where $S' = \frac{S}{\omega_s}$.

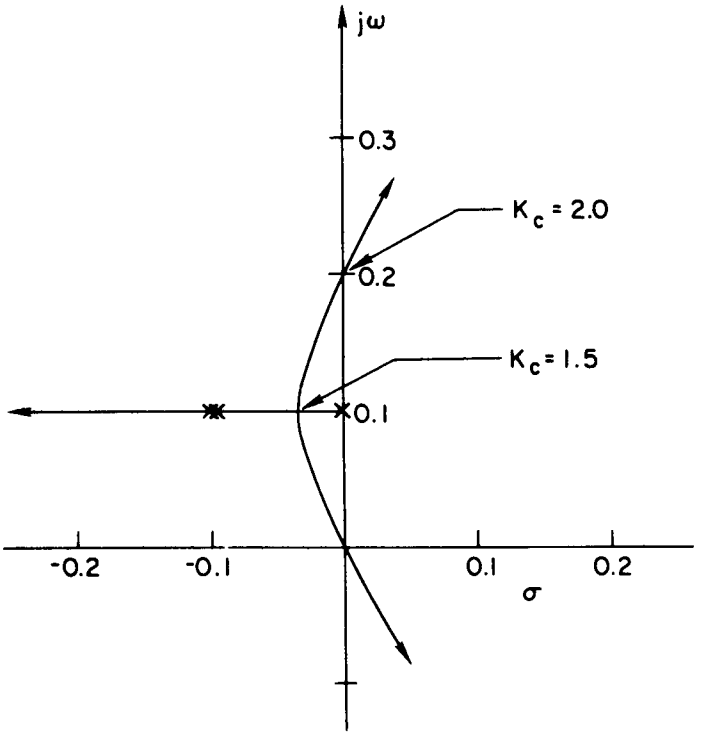

Fig. 6a. ROOT LOCUS PLOT VS K_c WITH

$\omega_s = 0.1$ rad/sec

$\gamma = 20$ sec

$K_p = 10^{-2}$ 1/sec^2

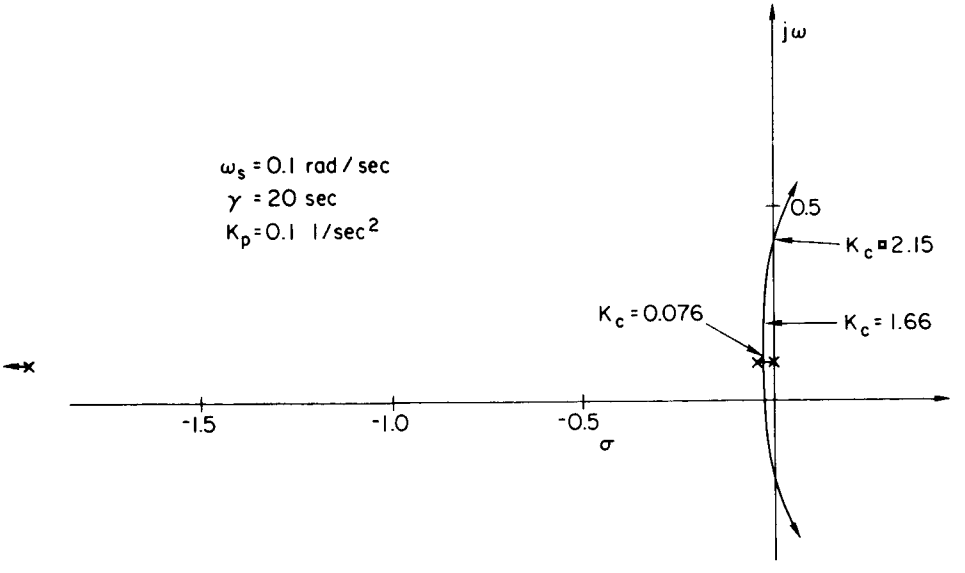

Fig. 6b. ROOT LOCUS VS K_c.

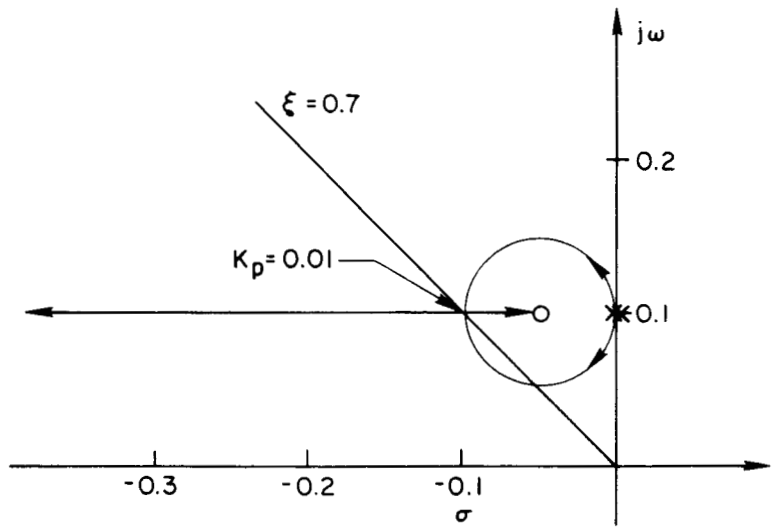

a. Root locus vs K_p ($\gamma\omega_s = 2$)

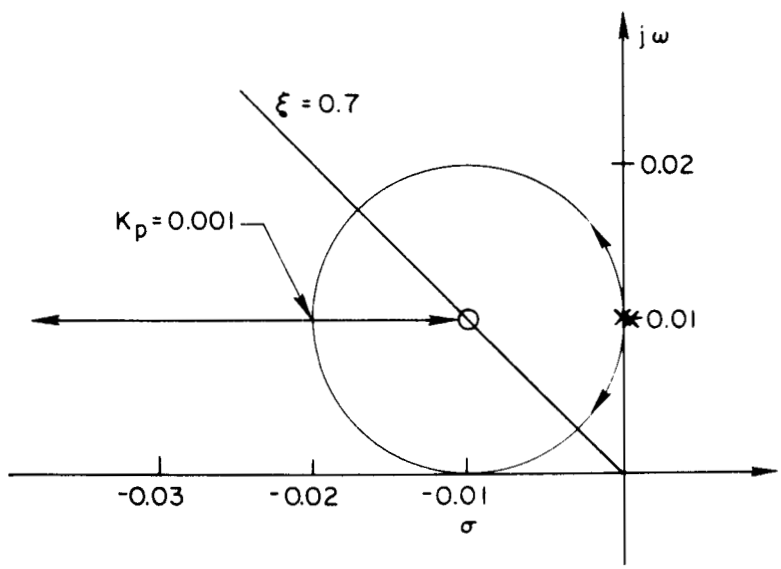

b. Root locus vs K_p ($\gamma\omega_s = 10$)
(note change in scale)

Fig. 7. NON-INTEGRAL CONTROLLER ROOT LOCUS PLOTS VS K_p.

To draw the root locus plot for an integral controller system:

a. Choose a value of $\gamma\omega_s$.

b. Pick a value of K_p from the non-integral controller plots such as given in Fig. 7. There will be two poles associated with this K_p.

c. The two poles found in (b) are the same as poles $S_{1,2}$ for the integral controller system.

d. Pole $S_3 = -j\omega_h$.

2. Computer Simulation of Integral Controller

To choose a range of acceptable K_c requires first choosing K_p and $\gamma\omega_s$. K_p is lower bounded by the fact that it must be large enough to move the proof mass away from the cavity wall if it were pushed against the wall at spinoff from the booster. This results in a criterion,

$$-f_c \cong K_p r_c > \omega_s^2 r_c$$

or

$$K_p > \omega_s^2 \tag{4.16}$$

where $r_c \triangleq$ radius of the satellite cavity.

$\gamma\omega_s$ is lower bounded ($\gamma\omega_s \gtrsim 1$), by two considerations. One, it must be high enough to provide sufficient damping. Two, it must be high enough to avoid being in the range of high susceptibility to "trapping", a fuel wasting limit cycle (see Chapter VI).

$\gamma\omega_s$ is upper bounded ($\gamma\omega_s \lesssim 3$) by stability considerations. As $\gamma\omega_s$ becomes larger, we see from Figs. 6 and 7 that the integral controller root locus is pushed more into the right half plane. Therefore, the range of stable K_c will be decreased.

Following the above guidelines, a typical set of parameters would be,

$$\omega_s = 0.1 \text{ rad/sec}$$

$$r_c = 3 \text{ mm}$$

$$\gamma = 20 \text{ sec}$$

$$K_p = 0.1 \text{ 1/sec}^2$$

$$r_d = 0.1 \text{ mm}$$

Figures 8 and 9 show the result of computer simulations of the integral controller with square deadspace [Eqs. (4.4a,b), (4.5a,b), and (4.8a,b) were simulated on both analog and digital computers using above values].

The computer simulations were done with a square deadspace controller, while the root locus analysis was done without a square deadspace. The results show that system behavior of the square deadspace integral controller can be predicted by the root locus plot of a controller without a deadspace.

On the basis of both analyses, only the following range of K_c should be considered for the system as described in this chapter,

$$10^{-2} > K_c > 8 \times 10^{-4} \text{ 1/sec}$$

C. On-Off Integral Controller with Square Deadspace

For actual application, on-off control (Fig. 10) will be used instead of linear control.* This section is intended to show that for the purpose of analyzing the integral controller, linear control is a very good approximation for on-off control.

Typical parameters for an on-off controller are,

$$\text{maximum control force} \triangleq f_m = 0.05 \text{ mm/sec}^2$$

$$r_d = 0.1 \text{ mm}$$

$$\text{minimum control impulse} \triangleq \Delta V = 0.001 \text{ mm/sec}$$

*The reason for this is that on-off controllers are less prone to control-gas leaks than linear controllers.

t (sec)	x_b (mm)	y_b (mm)	x_{bi} (mm)	y_{bi} (mm)
207.0	0.0229	0.0022	-0.0084	0.0213
208.0	0.0229	-0.0016	-0.0070	0.0218
209.0	0.0223	-0.0053	-0.0059	0.0219
210.0	0.0213	-0.0072	-0.0057	0.0217
211.0	0.0202	-0.0072	-0.0071	0.0203
212.0	0.0192	-0.0090	-0.0070	0.0199
213.0	0.0178	-0.0104	-0.0080	0.0178
214.0	0.0166	-0.0235	-0.0170	0.0020
215.0	0.0219	-0.1428	-0.1003	-0.1763
216.0	0.2546	-1.7200	-0.7856	-2.7470
217.0	5.3146	-22.5879	-3.3103	-38.5070
218.0	98.6120	-296.4783	54.4453	-518.1160
219.0	1683.6740	-3858.7380	2041.3030	-6717.0190
220.0	27286.2800	-49738.2300	44135.2300	-83674.6200
221.0	426655.5000	-634330.6000	797302.7000	-994660.5000
222.0	6496985.0000	**********	**********	**********
223.0	**********	**********	**********	**********
224.0	**********	**********	**********	**********
225.0	**********	**********	**********	**********
226.0	**********	**********	**********	**********
227.0	**********	**********	**********	**********
228.0	**********	**********	**********	**********
229.0	**********	**********	**********	**********
230.0	**********	**********	**********	**********
231.0	**********	**********	**********	**********
232.0	**********	**********	**********	**********
233.0	**********	**********	**********	**********

Fig. 8a. COMPUTER PRINTOUT OF UNSTABLE SYSTEM, K_c TOO HIGH.

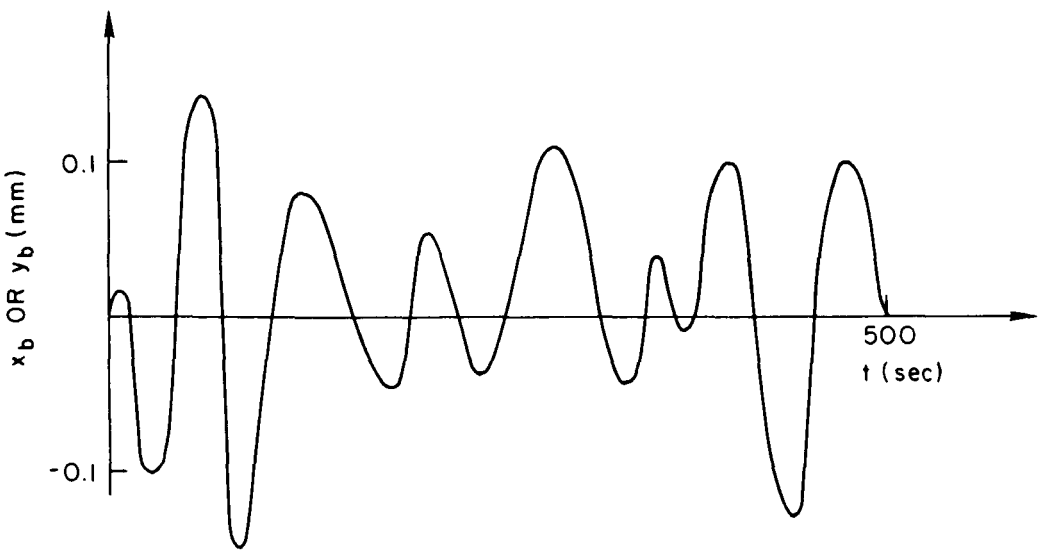

Fig. 8b. PLOT OF x_b OR y_b VS t, K_c TOO HIGH. Poles of the original non-integral system are displaced too much.

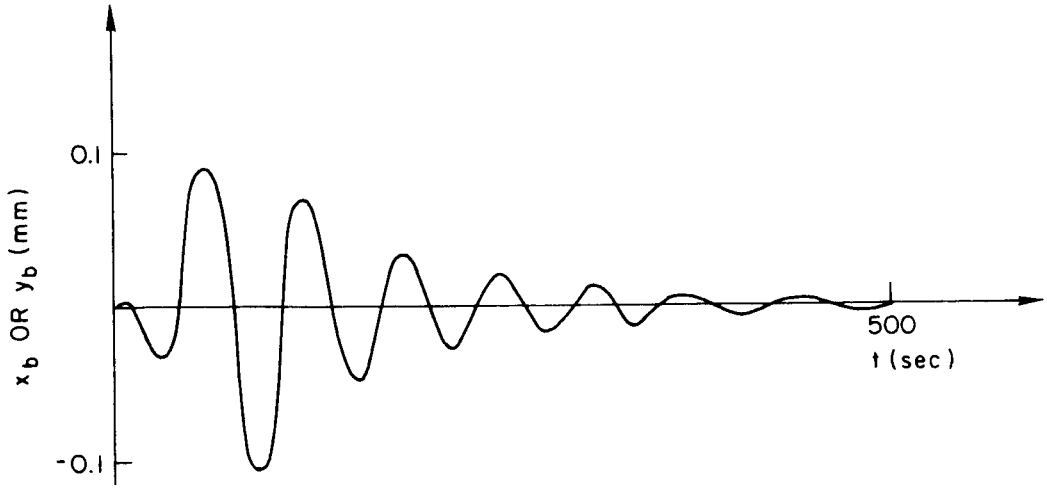

Fig. 8c. PLOT OF x_b OR y_b VS t. Optimal K_c.

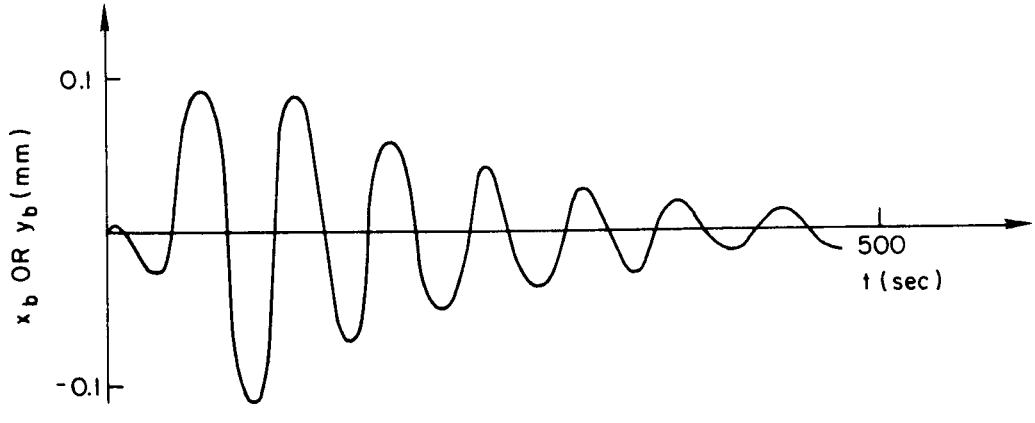

Fig. 8d. PLOT OF x_b/y_b VS t. Low K_c. Not enough damping.

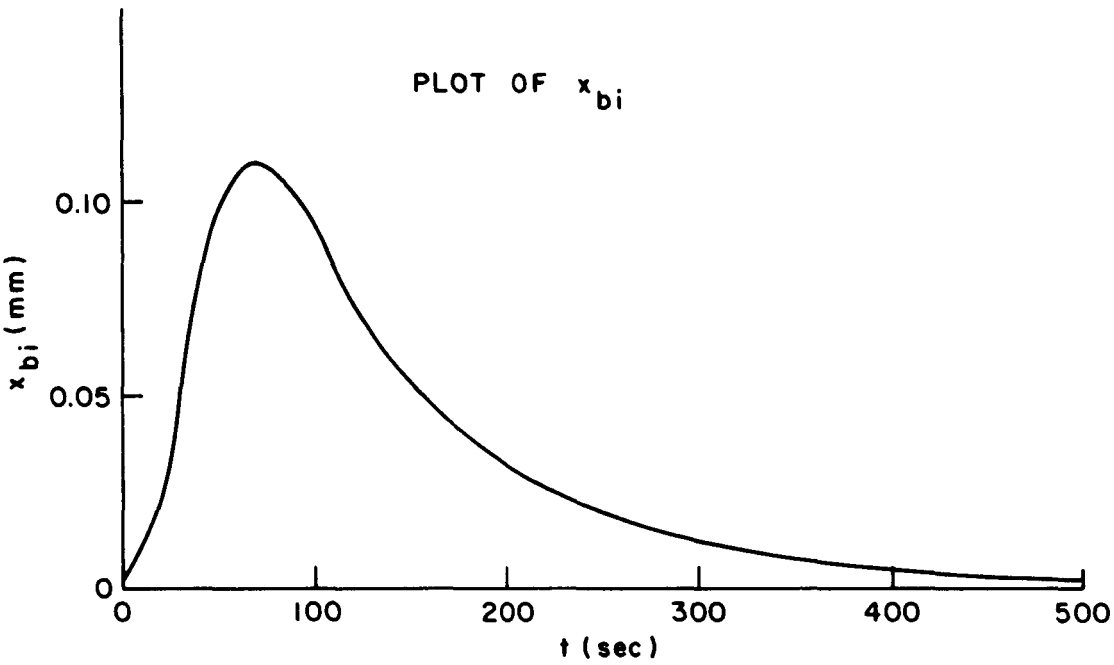

Fig. 9. PLOT OF x_{bi} VS t. x_{bi} is driven to zero, which implies that there is no mass attraction force.

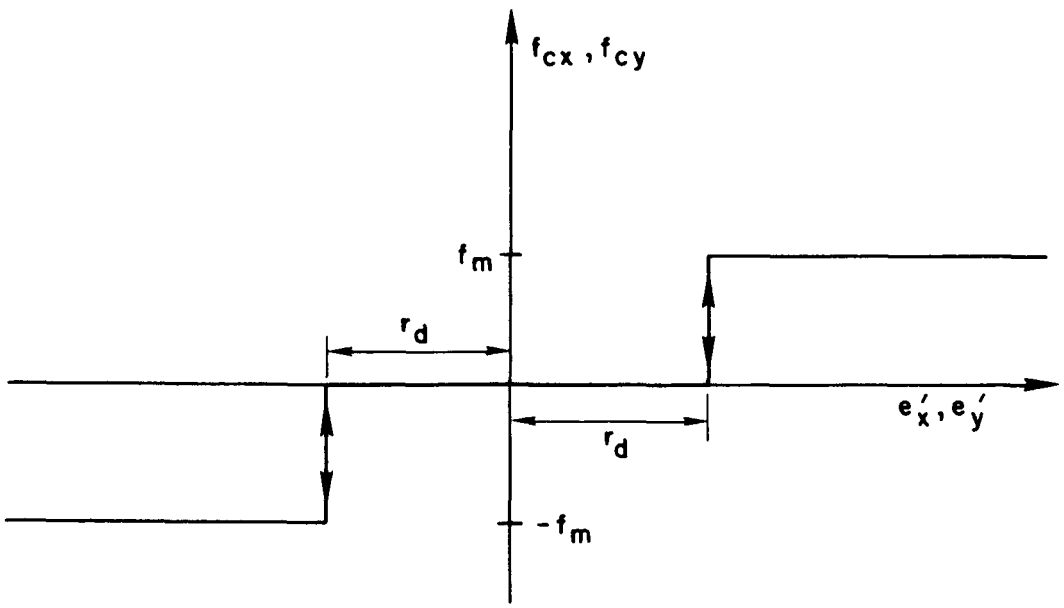

Fig. 10. ON-OFF CONTROLLER WITH SQUARE DEADSPACE.

Comparing Figs. 9 and 11, we see that on-off control behaves essentially as linear control does; except that x_{bi}, y_{bi} are not driven exactly to zero. This is expected, since the control force magnitude cannot be decreased, as needed when x_{bi} is very close to zero; and overshoot occures. This implies a non-zero average in-track mass attraction force, and will be discussed in the next chapter.

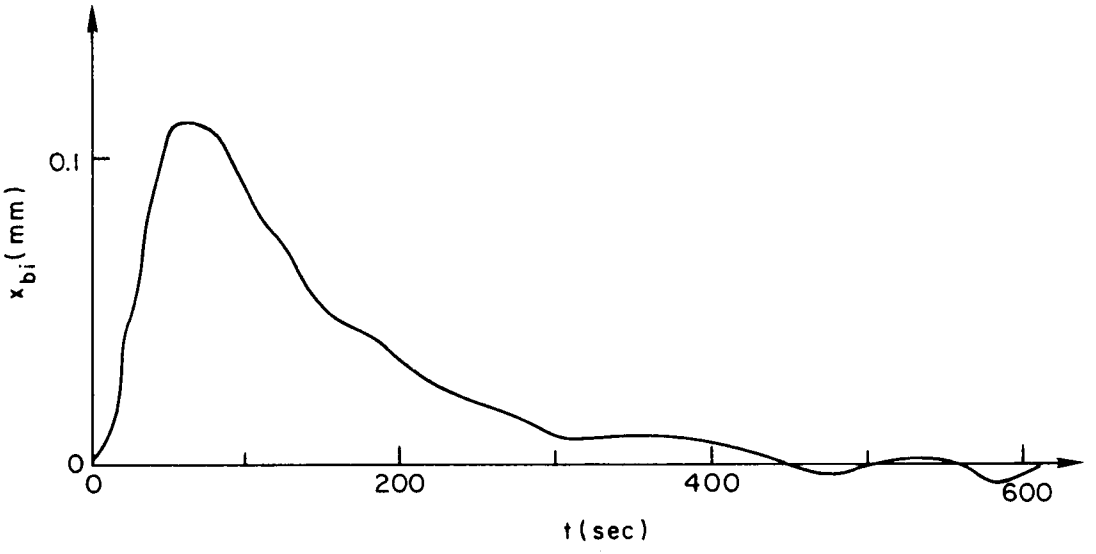

Fig. 11. PLOT OF x_{bi} VS t. [Equations (2.2a,b); (4.5a,b); and logic of Fig. 10 were simulated.]

D. On-Off Control with Octagonal Deadspace

For actual application, octagonal deadspace (Fig. 12) will be more likely used than square deadspace. This is because with an octagonal deadspace, there is better directional control on the control jets.

The following logic (Fig. 13) was used in the computer simulation,

$$\begin{aligned} a &\triangleq me'_y - e'_x \\ b &\triangleq e'_y - me'_x \qquad m = \tan\frac{\pi}{8} \\ c &\triangleq e'_y + me'_x \\ d &\triangleq me'_y + e'_x \end{aligned} \tag{4.17}$$

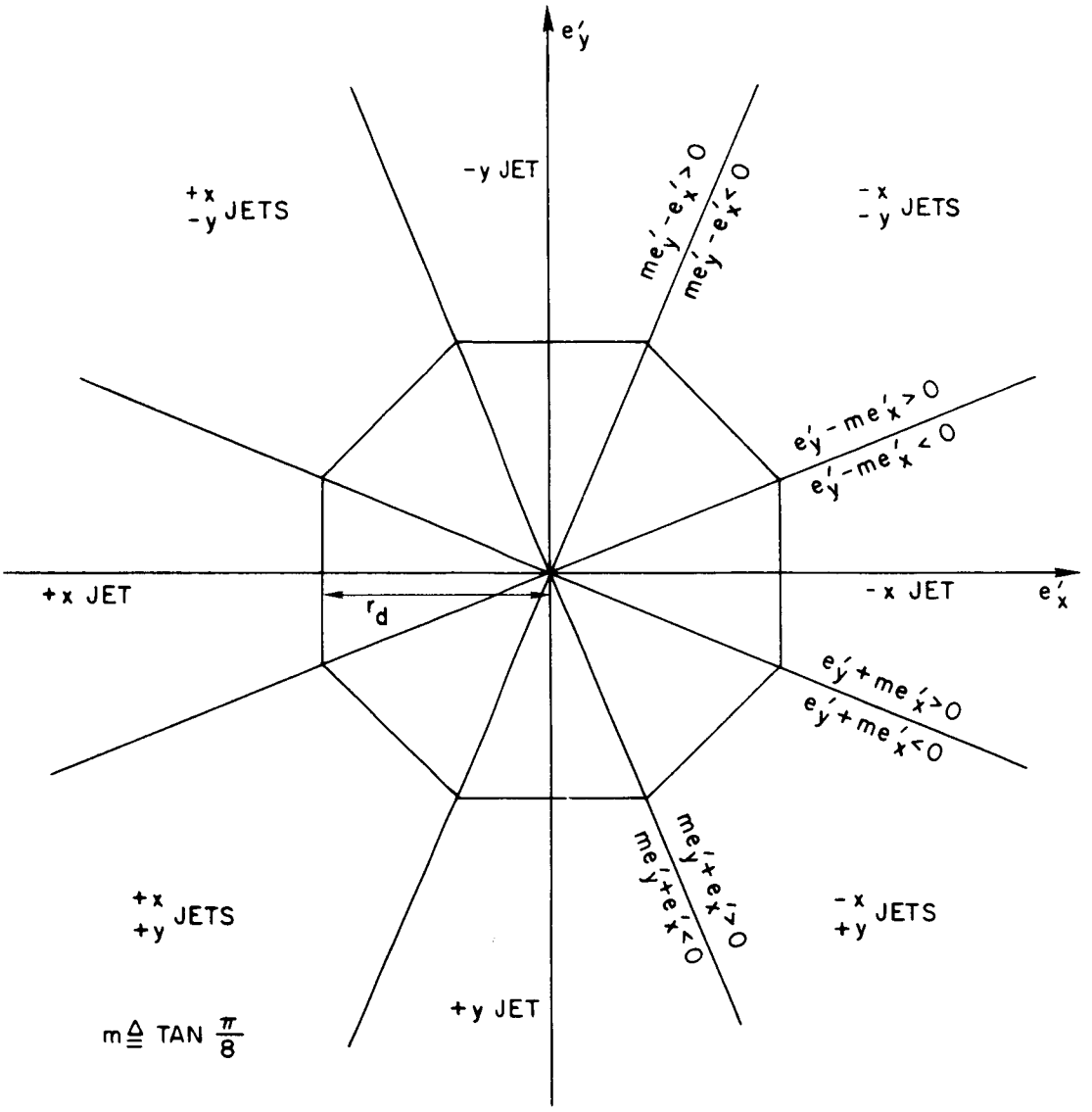

Fig. 12. OCTAGONAL DEADSPACE.

If		Switch Position
sgn(a) = sgn(d)	then	1
sgn(c) ≠ sgn(d)		2
sgn(a) ≠ sgn(b)		3
sgn(b) ≠ sgn(c)		4

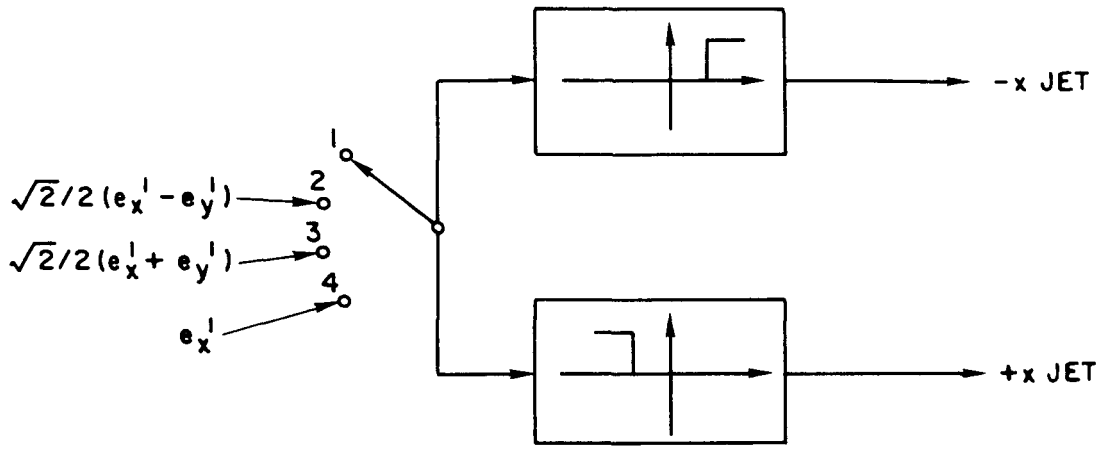

(a)

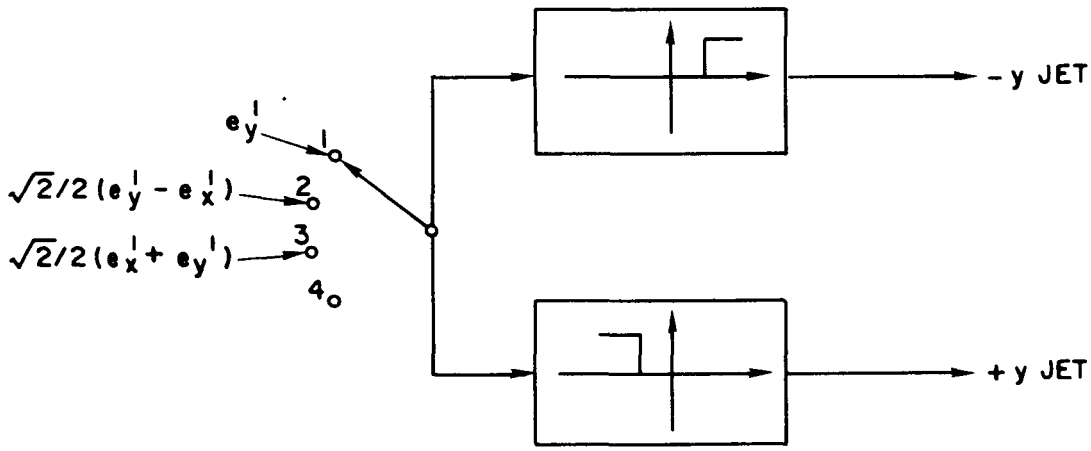

(b)

Fig. 13. OCTAGONAL DEADSPACE MECHANIZATION.

Comparing Figs. 11 and 14, we see that for the purposes of these analyses, linear control is also a good approximation of octagonal deadspace control. The "steady-state" x_{bi} oscillation amplitude is 2/3 that for the square deadspace, and this is expected since there is better directional control on the jets.

E. Conclusions

The stability of the control system with integral control has been analyzed. From root locus analysis of the linear integral controlled

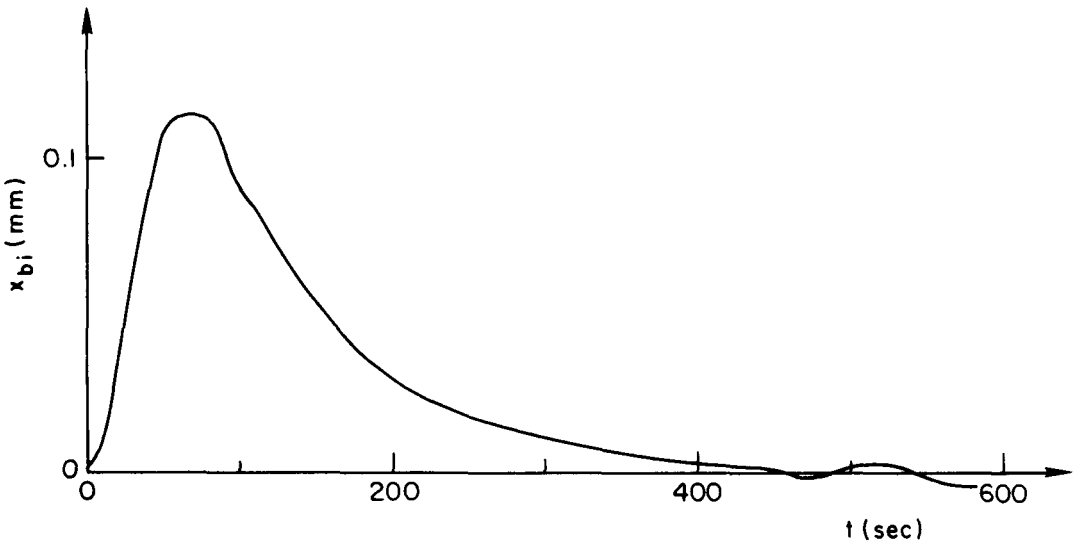

Using the same parameters as those used in the square deadspace simulation,

$$f_m = 0.05 \text{ mm/sec}^2$$

$$r_d = 0.1 \text{ mm}$$

$$\Delta V = 0.001 \text{ mm/sec}^2$$

Fig. 14. PLOT OF x_{bi} VS t. Computer simulation of system with octagonal deadspace controller. [Eqs. (2.2a,b) and logic of Fig. 13 were simulated.]

system without deadspace, coupled with knowledge of the basic non-integral controlled system, we can pick a range of acceptable K_c's for an on-off deadspace controller. For typical system parameters, the effect of varying K_c are,

(a) Very high K_c ($K_c \gtrsim 5$) - unstable.

(b) High K_c ($4 \gtrsim K_c \gtrsim 10^{-2}$) - poor performance because original control poles are disturbed.

(c) Optimal K_c ($10^{-2} \gtrsim K_c \gtrsim 8 \times 10^{-4}$)

(d) Low K_c ($8 \times 10^{-4} \gtrsim K_c$) - inadequate damping.

The effectiveness of this control law is discussed in the next chapter.

Chapter V

TRAJECTORY ERRORS WITH INTEGRAL CONTROL

The integral, on-off, deadspace controller reduces but does not eliminate average mass attraction force caused by a constant atmospheric drag. Mass attraction force can also be a result of the proof mass being in a limit cycle at certain specific frequencies, or of an inaccurately mechanized spin rate. These three error sources are described, and orders of magnitude for the errors calculated.

A. In-Track Trajectory Error Equations

Equation (3.2b) combined with Eq. (3.1a,b) can be rewritten as,

$$f_{eh} = cf_{ex_o} - sf_{ey_o} + Cx_{bi} + \Delta C(c_2 x_{bi} + s_2 y_{bi})$$

$$+ C_r(c_2 y_{bi} - s_2 x_{bi}) + \left(\text{terms with } \frac{\partial^n(\,)}{\partial x^n}\ c^i s^j x_{bi}^k y_{bi}^\ell\right.$$

$$\left.\text{where } n > 1,\ i + j > 2,\ k + \ell > 1\right) \qquad (5.1)$$

where

$$C \triangleq \frac{1}{2}\left(\frac{\partial f_{ex}}{\partial x} + \frac{\partial f_{ey}}{\partial y}\right)$$

$$\Delta C \triangleq \frac{1}{2}\left(\frac{\partial f_{ex}}{\partial x} - \frac{\partial f_{ey}}{\partial y}\right)$$

$$C_r \triangleq \frac{1}{2}\left(\frac{\partial f_{ex}}{\partial y} + \frac{\partial f_{ex}}{\partial x}\right)$$

$$s_2 \triangleq \sin(2\omega_h t) \qquad c_2 \triangleq \cos(2\omega_h t)$$

Lange [2] showed that in-track forces $f_{eh}(t)$ cause in-track trajectory errors $h(t)$ according to the Euler-Hill equation,

$$\frac{d^4h}{dt^4} + \omega_o^2 \frac{d^2h}{dt^2} = \frac{d^2 f_{eh}}{dt^2} - 3\omega_o^2 f_{eh} \qquad (5.2)$$

where

$$\omega_o \triangleq \text{ orbital rate} \approx 10^{-3} \text{ rad/sec}$$

For a constant f_{eh}, the solution to Eq. (5.2) is,

$$h(t) = \frac{f_{eh}}{\omega_o^2} \left\{ 4[1 - \cos(\omega_o t)] - \frac{3}{2} \omega_o^2 t^2 \right\} \qquad (5.3)$$

where $h(0) = 0$ $\dot{h}(0) = 0$.

B. Integral Controller Error

As was shown in Chapter IV-C & D, the integral controller with deadspace does not drive x_{bi}, y_{bi} to a "steady-state" value of zero. From Eq. (5.1), this implies a possible non-zero $\tilde{f}_{eh}$ (Fig. 15).

From Fig. 16, an $\tilde{f}_{eh}$ can be approximated by taking a time-weighted average slope of f_{eh}, beginning from $t = 750$ sec.

$$\tilde{f}_{eh} = \frac{1}{2} \times 10^{-14} \text{ g}$$

From Eq. (5.3),

$$h(t) = 2 \times 10^{-4}[1 - \cos(.001\, t)] - 0.75 \times 10^{-10}\, t^2$$

For long term effect, the first term can be neglected. The in-track trajectory error after one year is,

$$h = 72 \text{ m}$$

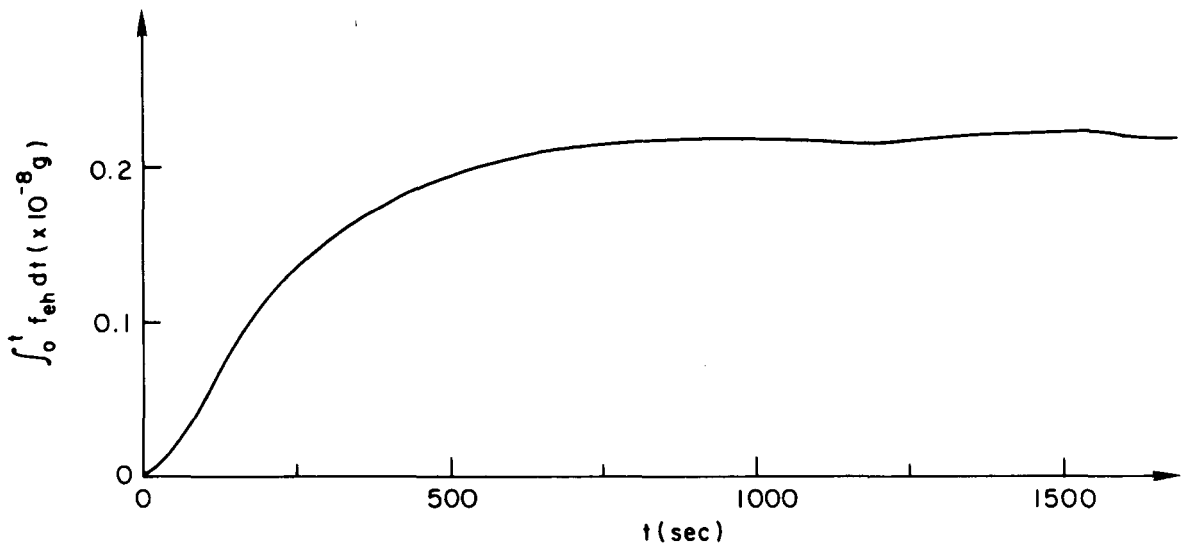

Fig. 15. PLOT OF $\int_0^t f_{eh}\,dt$ VS t. Computer simulation of system with on-off octagonal control, and simulation of f_{eh} and $\int f_{eh}$. [Eqs. (2.2a,b), (5.1) and logic of Fig. 13 were simulated.] The following parameters were used,

$$\omega_s = 0.1 \text{ rad/sec}$$

$$\gamma = 20 \text{ sec}$$

$$dV = 0.001 \text{ mm/sec}$$

$$f_m = 0.01 \text{ mm/sec}^2$$

$$r_d = 0.1 \text{ mm}$$

$$K_c = 0.004 \text{ 1/sec}$$

$$f_i = 10^{-3} \text{ mm/sec}^2$$

This is four orders of magnitude smaller than the in-track trajectory error without integral control, which was calculated by Powell [1] to be,

$$h = 150 \text{ km}$$

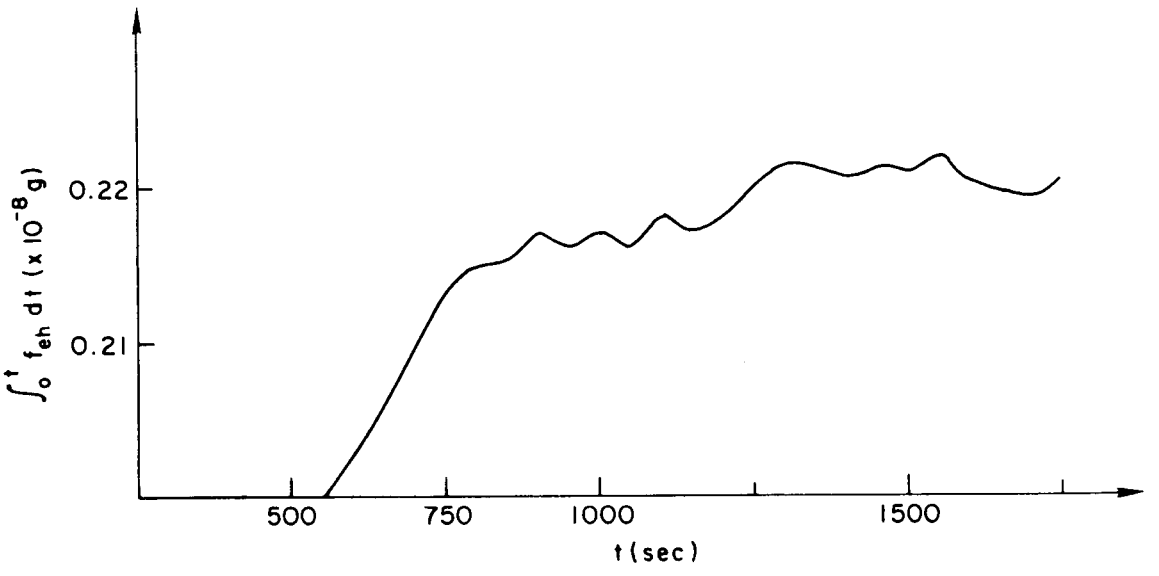

Fig. 16. ENLARGEMENT OF PORTION OF Fig. 15.

C. Error Due to Limit Cycling of the Proof Mass

From Eq. (5.1), we see that if $x_{bi}(t)$, $y_{bi}(t)$ were sinusoidal with certain frequencies (e.g., frequency = $2\omega_h$), $\tilde{f}_{eh}$ will be non-zero. Typical limit cycles with little or no external disturbance force is shown on the following page in Fig. 17.

$x_{bi}(t)$ and $y_{bi}(t)$ can be expanded in Fourier series,

$$x_{bi} = \sum_{j=0}^{\infty} a_j \cos (j\omega_{lc} t) \tag{5.4a}$$

$$y_{bi} = \sum_{j=0}^{\infty} a_j \sin (j\omega_{lc} t) \tag{5.4b}$$

where

$$a_j = \frac{2r_{lc}}{\pi^2 j^2} [-1 + (-1)^j] \tag{5.4c}$$

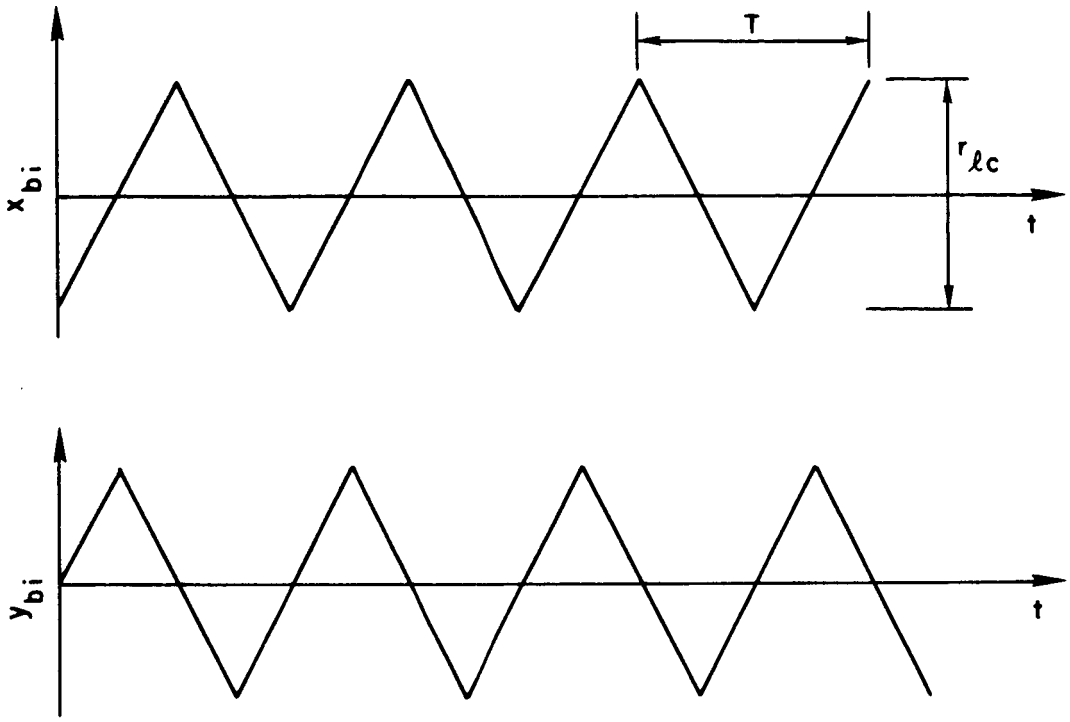

where

$$T = \frac{2\pi}{\omega_{1c}}$$

$$r_{1c} = 2r_d$$

Fig. 17. TYPICAL LIMIT CYCLES. Plots of x_{bi} and y_{bi} vs t.

Substituting Eqs. (5.4a,b) into Eq. (5.1),

$$f_{eh} = \left(cf_{ex_o} - sf_{ey_o}\right) + C\left[\sum_{j=0}^{\infty} a_j \cos(j\omega_{1c}t)\right]$$

$$+ \Delta C\left[c_2 \sum_{j=1}^{\infty} a_j \cos(j\omega_{1c}t) + s_2 \sum_{j=1}^{\infty} a_j \sin(j\omega_{1c}t)\right]$$

$$+ C_r\left[c_2 \sum_{j=1}^{\infty} a_j \sin(j\omega_{1c}t) - s_2 \sum_{j=1}^{\infty} a_j \cos(j\omega_{1c}t)\right]$$

$$+ \ldots \qquad (5.5)$$

Since the only significant in-track error is caused by a non-zero $\tilde{f}_{eh}$, we note that $\tilde{f}_{eh}$ is significant only when x_{bi}, y_{bi} are oscillating at certain frequencies.

$$\tilde{f}_{eh} = \Delta C a_j \qquad \text{if} \quad j\omega_{lc} = 2\omega_h$$

$$\tilde{f}_{eh} = \frac{1}{32} \frac{\partial^2 f_{ex}}{\partial x^2} a_j \qquad \text{if} \quad j\omega_{lc} = \frac{3}{2}\omega_h$$

$$\tilde{f}_{eh} = \frac{3}{32} \frac{\partial^2 f_{ex}}{\partial x^2} a_j \qquad \text{if} \quad j\omega_{lc} = \frac{1}{2}\omega_h \tag{5.6}$$

$$\vdots \qquad\qquad \vdots$$

The largest of these errors occur when $j\omega_{lc} = 2\omega_h$. It is of interest to see what the error is when

$$j\omega_{lc} = 2\omega_h + \epsilon \tag{5.7}$$

assuming $\epsilon \ll \omega_h$.

Equation (5.5) becomes,

$$f_{eh} = a_j [\Delta C \cos(\epsilon t) + C_r \sin(\epsilon t)]$$

$$+ \text{sinusoidal terms with frequencies} \gg \omega_o \tag{5.8}$$

The terms with frequencies much higher than ω_o do not contribute significant in-track trajectory errors. Therefore, Eq. (5.8) can be rewritten as,

$$f_{eh} \approx K_j [\cos(\epsilon t) + \sin(\epsilon t)] \tag{5.9}$$

where

$$*\Delta C = C_r = 10^{-10} \text{ g/mm}$$

$$K_j \triangleq 10^{-10} a_j$$

Substituting this in Eq. (5.2),

$$\frac{d^4h}{dt^4} + \omega_o^2 \frac{d^2h}{dt^2} = -K_j \left(\epsilon^2 + 3\omega_o^2\right) [\cos(\epsilon t) + \sin(\epsilon t)] \qquad (5.10)$$

Solving this with initial conditions $h(0) = 0$, $h'(0) = 0$, $h''(0) = 0$, $h'''(0) = 0$, we get,

$$h(t) = \frac{k_j\left(\frac{\epsilon^2}{\omega_o^2} + 3\right)}{\left(\epsilon^2 \frac{\epsilon^2}{\omega_o^2} - 1\right)} \left\{ \left(1 - \frac{\epsilon^2}{\omega_o^2}\right) + \epsilon\left(1 - \frac{\epsilon^2}{\omega_o^2}\right)t \right.$$

$$\left. + \frac{\epsilon^2}{\omega_o^2} \cos(\omega_o t) + \frac{\epsilon^3}{\omega_o^3} \sin(\omega_o t) - \cos(\epsilon t) - \sin(\epsilon t) \right\} \qquad (5.11)$$

For $\epsilon \ll \omega_o$ (this assumption will be shown to be valid),

$$h(t) \approx -\frac{3K_j}{\epsilon} \{1 + \epsilon t - \cos(\epsilon t) - \sin(\epsilon t)\} \qquad (5.12)$$

Expanding $\cos(\epsilon t)$ and $\sin(\epsilon t)$ in Taylor series,

$$h(t) = -\frac{3}{2} K_j t^2 - 3K_j \left[\frac{\epsilon t^3}{3!} - \frac{\epsilon^2 t^4}{4!} - \frac{\epsilon^3 t^5}{5!} + \ldots\right] \qquad (5.13)$$

*Since ϵ can be either positive or negative, the sign of C_r and ΔC in Eq. (5.9) does not matter.

If

$$\epsilon = 0, \quad h(t) = -\frac{3}{2} K_j t^2 \tag{5.14}$$

Rewriting Eq. (5.13),

$$\frac{h(t)}{-\frac{3}{2} K_j t^2} = 1 + \frac{1}{3}\epsilon t - \frac{1}{12}\epsilon^2 t^2 - \frac{1}{60}\epsilon^3 t^3 + \frac{1}{360}\epsilon^4 t^4 + \frac{1}{2520}\epsilon^5 t^5 - \frac{1}{20,160}\epsilon^6 t^6 - \frac{1}{181,440}\epsilon^7 t^7 + \text{h.o.t.} \tag{5.15}$$

Plotting Eq. (5.15) for $|\epsilon t| \leq 3$, the higher order terms can be neglected. From Fig. (18), we see that,

$$\left(\frac{h(t)}{-\frac{3}{2} K_j t^2}\right)_{max} = 1.27 \quad \text{at} \quad \epsilon t \approx 1.6 \text{ rad} \tag{5.16}$$

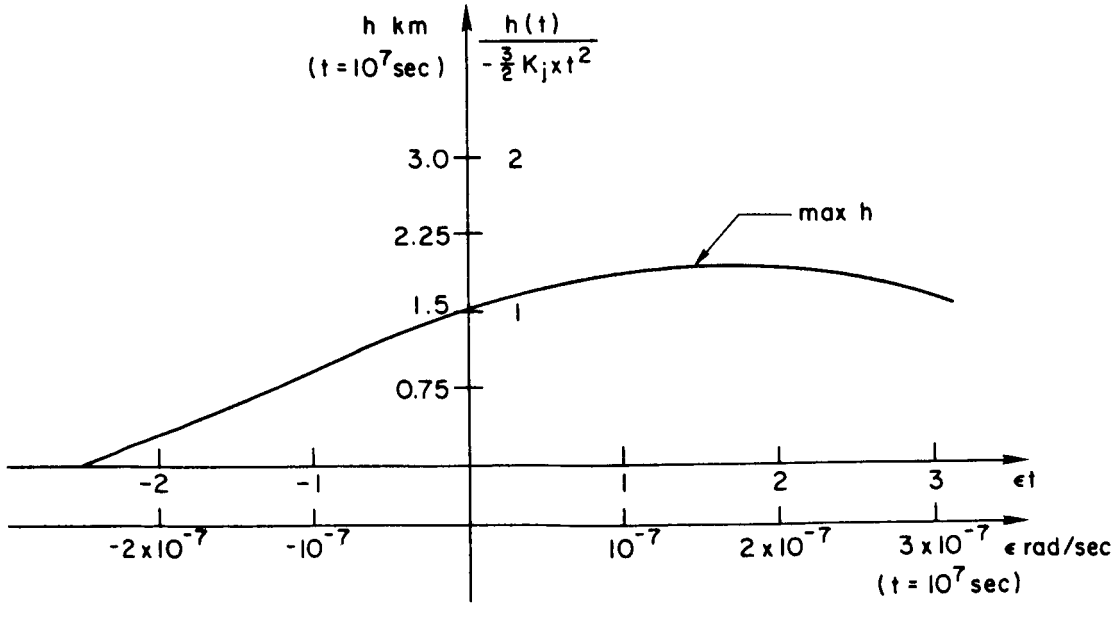

Fig. 18. PLOT OF $[h(t)/(-3/2\ K_j t^2)]$ VS ϵt; AND h VS ϵ FOR $t = 10^7 (\approx 4$ MONTHS) (ASSUMING THAT $3\omega_{1c} = 2\omega_h + \epsilon$).

This implies that after 4 months (10^7 sec), with $\epsilon = 1.6 \times 10^{-7}$ rad/sec,

$$|h|_{max} = 19 \text{ km} \quad \text{if} \quad \omega_{lc} = 2\omega_h + \epsilon$$

$$K_1 = 10^{-6} a_1$$

and

$$|h|_{max} = 1.9 \text{ km} \quad \text{if} \quad 3\omega_{lc} = 2\omega_h + \epsilon$$

$$K_3 = 10^{-6} a_3$$

The limit cycle frequency is determined by the following equation [1], for a given satellite,

$$\omega_{lc} = \frac{\pi}{4} \frac{\Delta V}{r_d}$$

Typically, $5 \times 10^{-3} > \Delta V > 5 \times 10^{-4}$ mm/sec, corresponding to $f_m = 0.05$ mm/sec^2 and $0.1 > \Delta t > 0.01$ msec. These values of ΔV give $0.05 \gtrsim \omega_{lc} \gtrsim 0.005$ rad/sec, and

$$|\epsilon| \gtrsim 0.15 \text{ rad/sec} \quad \text{if} \quad \omega_{lc} = 2\omega_k + \epsilon$$

$$|\epsilon| \gtrsim 0.05 \text{ rad/sec} \quad \text{if} \quad 3\omega_{lc} = 2\omega_h + \epsilon$$

$$|\epsilon| \gtrsim 0.05 \text{ rad/sec} \quad \text{if} \quad 5\omega_{lc} = 2\omega_h + \epsilon$$

Higher order terms can be neglected since h is proportional to a_j, which is inversely proportional to j^2. Therefore, ϵ can be expected to be greater than 10^{-2} rad/sec; and the behavior of h at ϵ of the order of 10^{-7} rad/sec is purely academic.

It remains now to analyze the behavior of h as ϵ increases. Equations (5.12) can be approximated by,

$$h(t) = -\frac{3K_j}{\epsilon} t \quad \text{if} \quad \epsilon t \gg 1 \tag{5.17}$$

For a given t, h decreases as ϵ increases. With $t = 4$ months (10^7 sec), and $|\epsilon| = 10^{-5}$ rad/sec,

$$|h| = 3 \times 10^4 \text{ mm} = 30 \text{ m} = 2\% \text{ of } |h_{max}| \quad \text{if} \quad 3\omega_{1c} = 2\omega_h + \epsilon$$

(Note that the assumption that $\epsilon \ll \omega_o$ has now been shown to be valid.)

The fact that h_{max} does not occur precisely at resonance was not expected. Looking back at Eq. (5.5), we see that at resonance, the non-zero contributions to $\tilde{f}_{eh}$ are from terms of c_2^2, s_2^2 ($c_2 \cdot \cos[(2\omega_h + \epsilon)t]$, $s_2 \cdot \sin[(2\omega_h + \epsilon)t]$ if not in perfect resonance) (Fig. 19a,b).

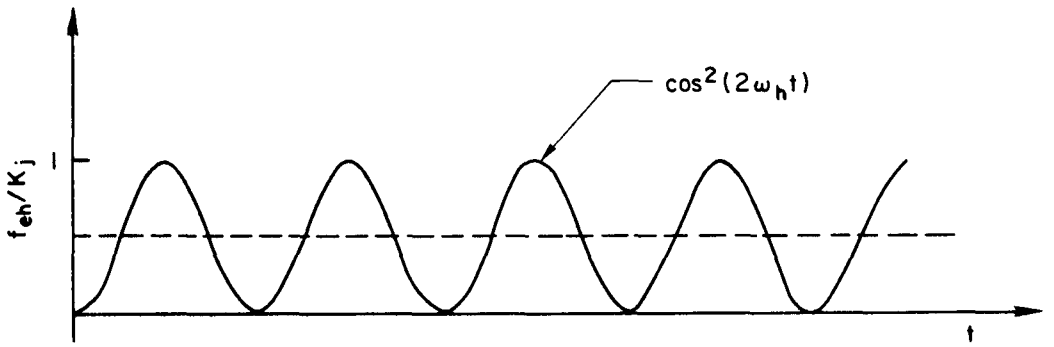

Fig. 19a. PLOT OF $f_{eh}(t)$ AT RESONANCE. Dotted line show average of $\cos^2(2\omega_h t)$.

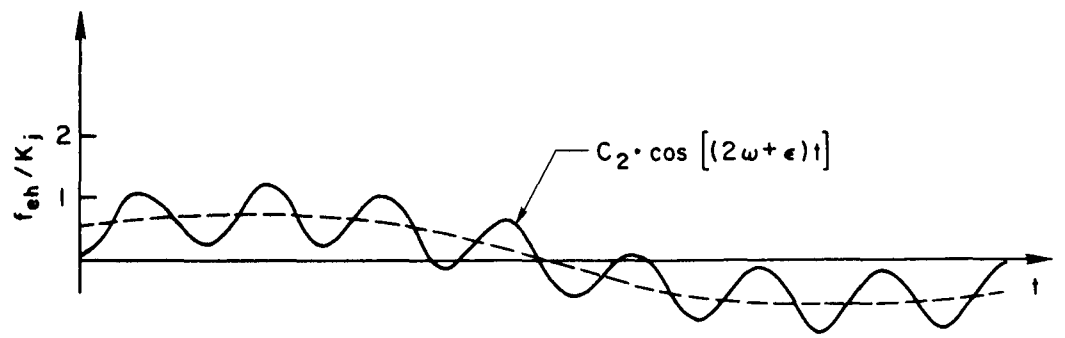

Fig. 19b. PLOT OF $f_{eh}(t)$ CLOSE TO RESONANCE. Dotted line show average of $\cos(2\omega_h t) \cdot \cos[(2\omega_h + \epsilon)t]$, and is a sine curve with frequency ϵ.

At resonance, $\tilde{f}_{eh}$ is a constant; while close to resonance, it is a sine wave with frequency ϵ. Therefore, with certain ϵ's, in-track

trajectory errors will actually be bigger than if the limit cycle were in perfect resonance.

In computer simulations, it was found that limit cycles with ω_{lc} greater than ω_h can not be simulated. This can be explained by the fact that with $\omega_{lc} > \omega_h$, correct (on-off) jet alignment to perpetuate a limit cycle is impossible. (See. Fig. 20.) Therefore, the largest error would be caused by limit cycles with frequency $3\omega_{lc} = 2\omega + \epsilon$.

It was also found that even though limit cycles at frequency $3\omega_{lc} = 2\omega$ can be simulated, limit cycles at frequency $3\omega_{lc} = 2\omega + \epsilon$ cannot be sustained. Again this can be explained by the fact that the on-off jets can not continuously produce pulses in the correct direction (Fig. 20).

The conclusion is that the worst error that will occur will be from limit cycles of frequency $\omega_{lc} = 2/3\ \omega_h$, which gives an in-track trajectory error of 1.5 km if allowed to limit cycle for 4 months. The errors from limit cycles close to resonance frequency will not be significant since on-off control will not sustain such limit cycles.

D. Spin Rate Error

The integral controller is mechanized by introducing a control center bias x_u, y_u as shown in Chapter IV-1. This involves mechanizing a spin rate of ω_h. If this mechanized spin rate, $\bar{\omega}_h$, is not equal to ω_h, the controller senses a local horizontal which is rotating with respect to the actual local horizontal. This results in the controller sensing any constant horizontal displacement (such as that caused by constant atmospheric drag), as a rotating disturbance.

Equations (4.1) and (4.2) can be rewritten as,

$$\begin{bmatrix} x_u \\ y_u \end{bmatrix} = -K_c \begin{bmatrix} \bar{c} & -\bar{s} \\ \bar{s} & \bar{c} \end{bmatrix}^{-1} \begin{bmatrix} I_{hc} \\ I_{vc} \end{bmatrix} \qquad (5.18a)$$

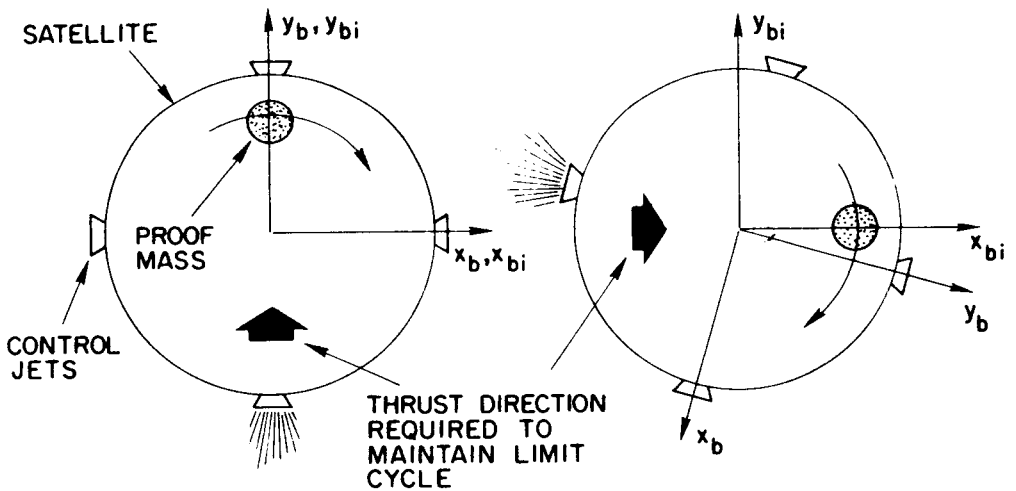

Fig. 20. LACK OF DIRECTIONAL CONTROL WITH ON-OFF OCTAGONAL DEADSPACE CONTROLLER, (ASSUME $\omega_{lc} = 5/6\ \omega_h$).

$$\begin{bmatrix} I_{hc} \\ I_{vc} \end{bmatrix} = \int_0^t \begin{bmatrix} \bar{c} & -\bar{s} \\ \bar{s} & \bar{c} \end{bmatrix} \begin{bmatrix} x_b \\ y_b \end{bmatrix} dt \qquad (5.18b)$$

where

$$\bar{c} = \cos(\bar{\omega}_h t)$$

$$\bar{s} = \sin(\bar{\omega}_h t)$$

Using the average values of f_{eh} from Fig. 21, we find the in-track errors after one year are,

h = 72 m if $|\omega_h - \bar{\omega}_h| = 0$

h = 908 m if $|\omega_h - \bar{\omega}_h| = 0.001$

h = 4.05 km if $|\omega_h - \bar{\omega}_h| = 0.003$

h = 5.4 km if $|\omega_h - \bar{\omega}_h| = 0.004$

h = 9.45 km if $|\omega_h - \bar{\omega}_h| = 0.006$

E. Conclusions

An analysis has been made on three sources of trajectory errors, with the mechanization of integral control. The integral controller will reduce in-track trajectory errors caused by mass attraction force from 150 km to 72 m, after 1 year.

Limit cycles will cause maximum trajectory error if the frequency is approximately 10^{-7} rad/sec away from resonance frequency. This h_{max} (≈ 1.9 km) is from the highest resonance frequency possible with on-off control ($3\omega_{lc} = 2\omega_h$). Higher resonance frequencies are not obtainable, because of the lack of directional control on the control jets.

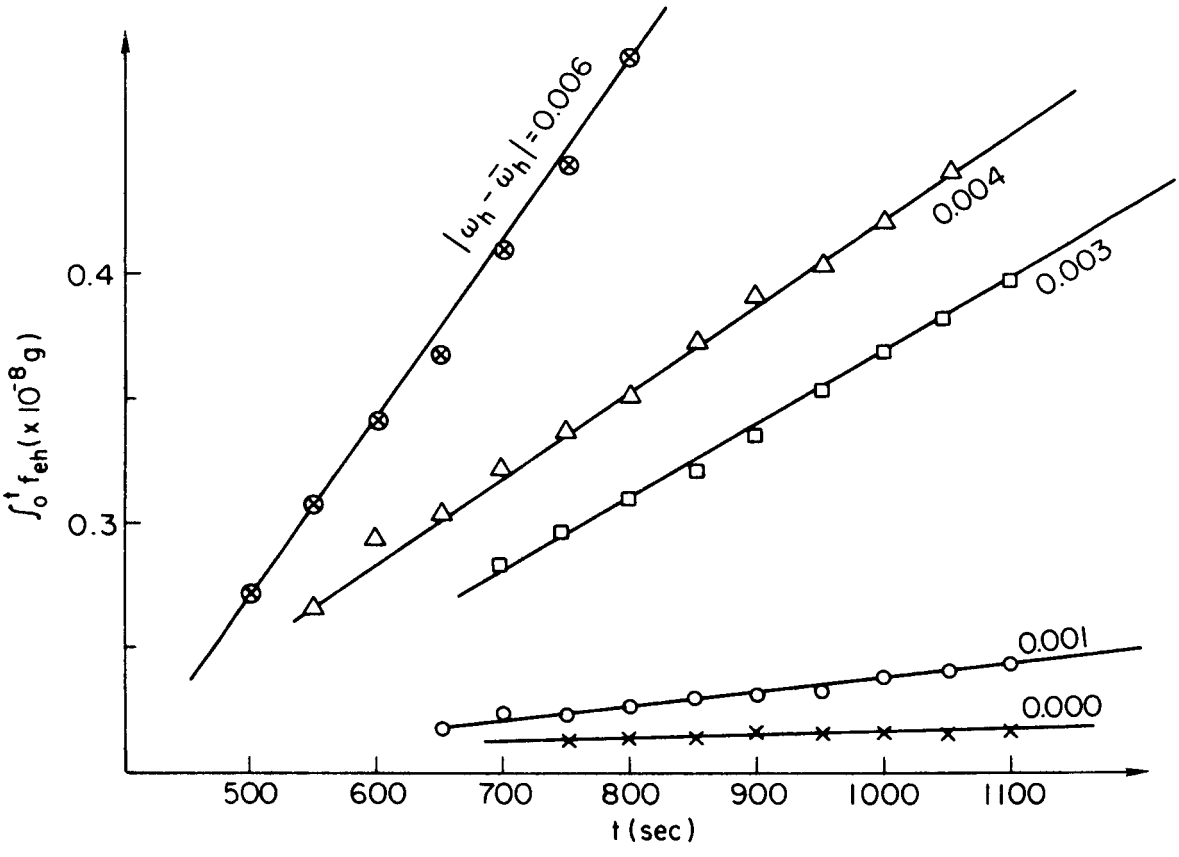

This was mechanized in the computer with the following input values

$dV = 0.001$ mm/sec

$f_m = 0.01$ mm/sec^2

$r_d = 0.1$ mm

$\gamma = 20$ sec

$K_c = 0.004$ 1/sec

$\omega_s = 0.1$ rad/sec

$\omega_o = 0.001$ rad/sec

$\bar{\omega}_h = 0.095, 0.099, 0.100, 0.102, 0.105$ rad/sec

$f_i = 10^{-3}$ mm/sec^2

Fig. 21. $\int_0^t f_{eh}\, dt$ VS t FOR VARIOUS VALUES OF $|\omega_h - \bar{\omega}_h|$.

With an $|\epsilon|$ of 10^{-5} rad/sec, $|h|$ is already down to 2% of $|h_{max}|$. For typical control impulse sizes ($5 \times 10^{-3} > \Delta V > 5 \times 10^{-4}$ mm/sec), $|\epsilon|$ is greater than 10^{-2} rad/sec. Therefore, error caused by limit cycle is negligible.

Chapter VI

TRAPPING SUSCEPTIBILITY

The "trapping" phenomenon is described. Trapping susceptibility of circular versus square deadspace, and trapping susceptibility versus K_p/ω_s^2 are analyzed.

A. Description of Trapping

Trapping, a phenomenon first described by Powell [1], occurs when the proof mass is in a stable equilibrium position outside the deadspace. This results in the constant expenditure of fuel while little or no external force is present.

This phenomenon was encountered during the study of limit cycle errors, when it was necessary to simulate limit cycles of certain resonant frequencies. It was found that limit cycles with $\omega_{lc} = \omega_s$ were particularly easy to simulate. This implied that the proof mass was prone to be "trapped" in a fixed position in the satellite frame of reference.

B. Trapping Susceptibility

Equilibrium positions of the proof mass can be found by solving the following equations [1],

$$\frac{\omega_s^2}{K_p}(x_b - x_e) = x_b - \gamma\omega_s y_b - \frac{x_b - \gamma\omega_s y_b}{\sqrt{\left(1 + \gamma^2\omega_s^2\right)\left(x_b^2 + y_b^2\right)}} \tag{6.1a}$$

$$\frac{\omega_s^2}{K_p}(y_b - y_e) = y_b + \gamma\omega_s x_b - \frac{y_b + \gamma\omega_s x_b}{\sqrt{\left(1 + \gamma^2\omega_s^2\right)\left(x_b^2 + y_b^2\right)}} \tag{6.1b}$$

which are the steady state solutions to Eq. (2.4). These can be transformed into polar coordinates,

$$x_b = r_b c$$

$$y_b = r_b s$$

where

$$c \triangleq \cos\theta$$

$$s \triangleq \sin\theta$$

$$r_b \triangleq \sqrt{x_b^2 + y_b^2}$$

Equations (6.1a,b) become,

$$f(\theta) \triangleq \frac{r_d}{\beta}\delta\eta + \eta x_e(\eta s - s - \delta c) - \eta y_e(\eta c - c + \delta s) = 0 \qquad (6.2)$$

where

$$\delta \triangleq \gamma\omega_s$$

$$\eta \triangleq \omega_s^2/K_p$$

$$\beta \triangleq \sqrt{1 + \gamma^2\omega_s^2}$$

An existing program [1] which solved Eq. (6.2) and checked the stability of the solutions was used and the results shown in Fig. 22. Since $r^*(\text{circular}) > r^*(\text{square})$, the circular deadspace is less susceptible to trapping than the square deadspace.

In the initial analog simulations for this study, a $K_p/\omega_s^2 < 1$ was used because of overloading problems on the computer. It was found that the system was less prone to being trapped than when a $K_p/\omega_s^2 > 1$ was used. An analysis of r^* versus K_p/ω_s^2 was made and the result is shown in Fig. 23. Powell [1] had shown, for $K_p/\omega_s^2 = 15$, that optimal r^* occurred at $\gamma\omega_s = 1$ and $\gamma\omega_s = 2.4$ for the circular and square deadspaces, respectively. In simulations, this has been shown to be true in general.

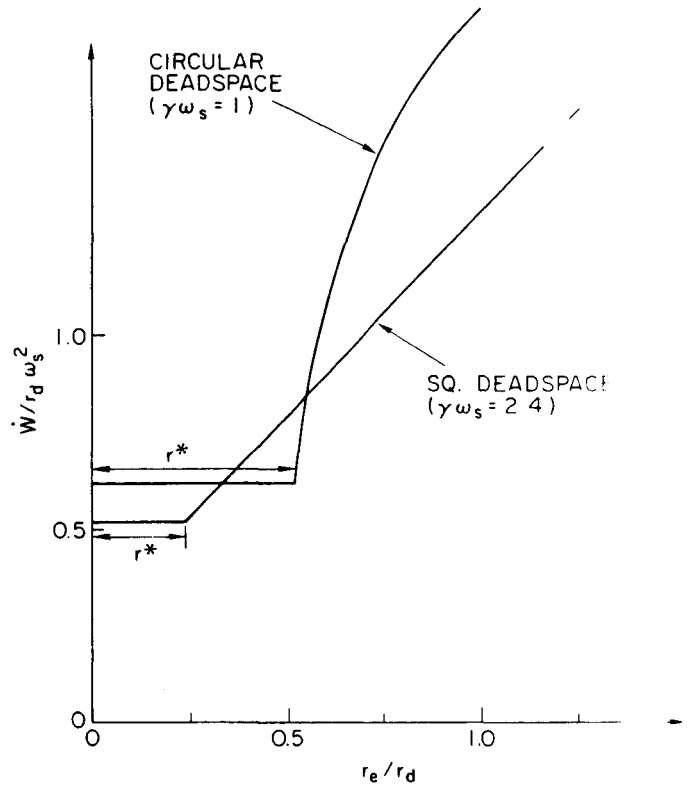

Fig. 22. CONTROL EFFORT VS CENTER OF MASS FOR $K_p/\omega_s^2 = 10$.

Figure 24 shows the amount of fuel wasted versus K_p/ω_s^2.

C. Conclusions

For $K_p/\omega_s^2 > 1$, which will be required in a real system [see Eq. (4.16)], circular deadspace is less susceptible to trapping than square deadspace. For $K_p/\omega_s^2 < 1$, r^* rises significantly as K_p/ω_s^2 is decreased. However, for $K_p/\omega_s^2 > 1$, no significant gain in trapping susceptibility will be made by changing K_p/ω_s^2.

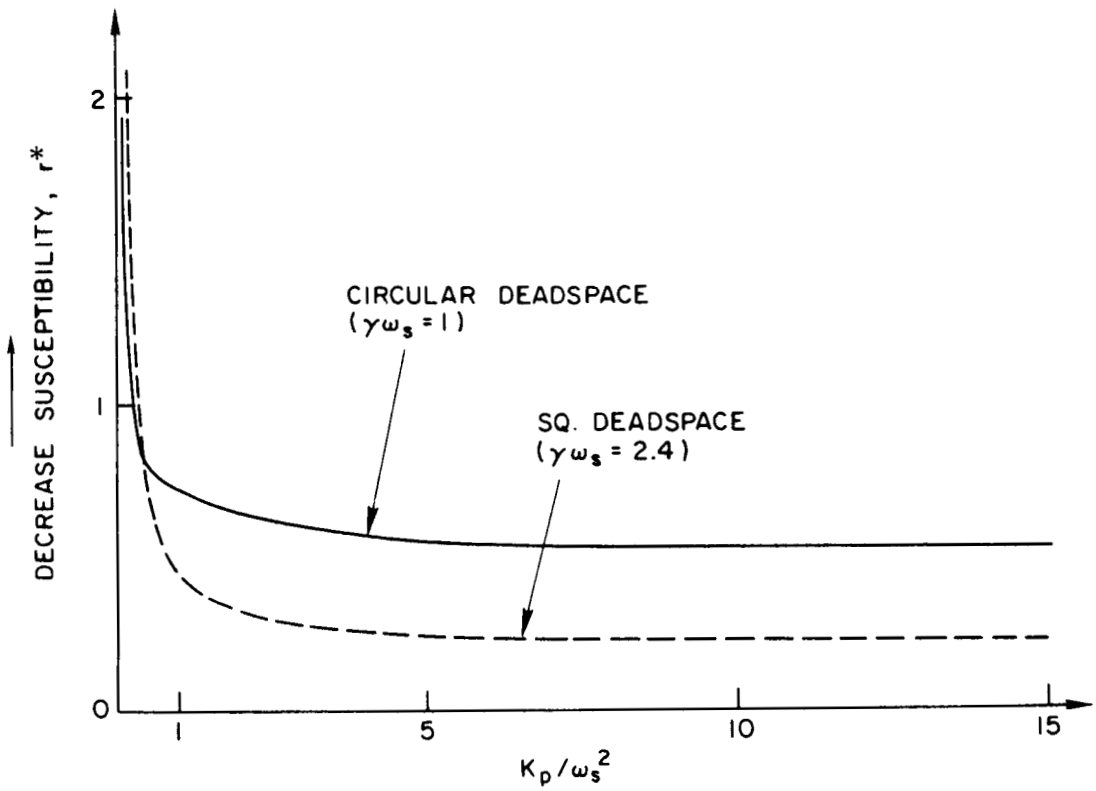

Fig. 23. TRAPPING SUSCEPTIBILITY VS K_p/ω_s^2.

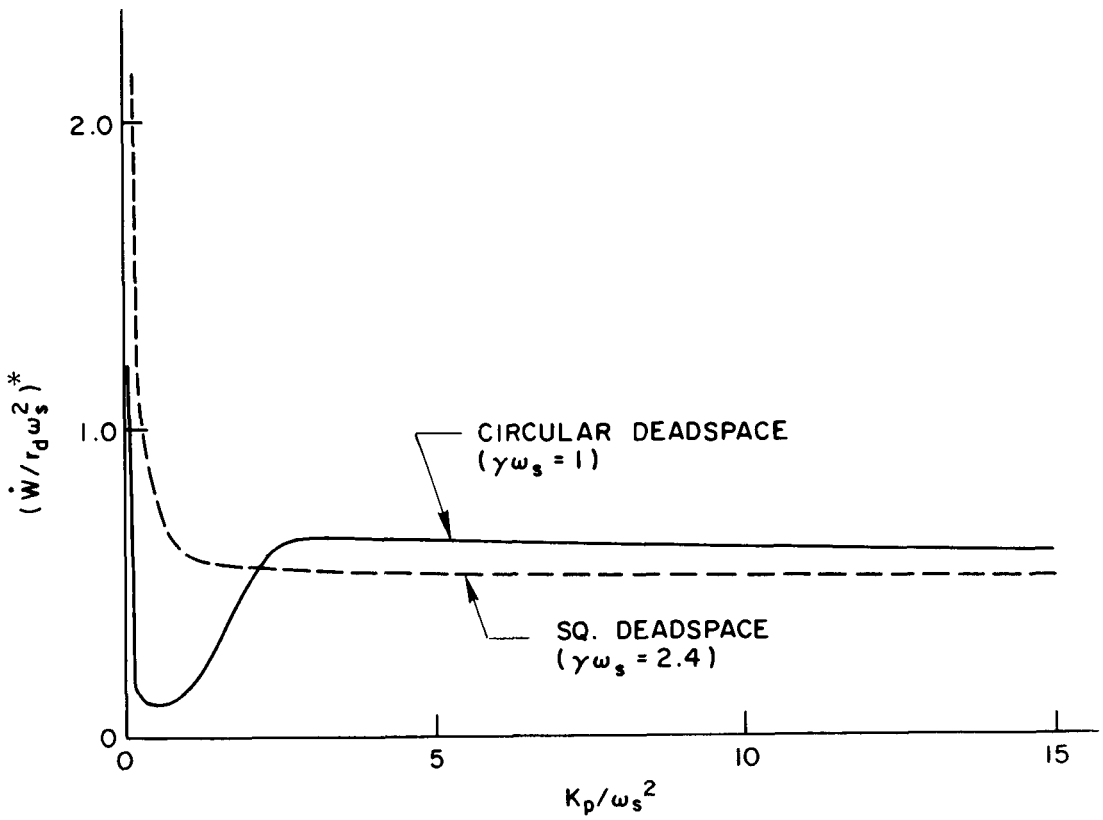

Fig. 24. $(\dot{W}/r_d\omega_s^2)^*$, A MEASURE OF THE FUEL RATE AT TRAPPED SOLUTION (i.e., $r_e/r_d = r^*$), VS K_p/ω_s^2.

Chapter VII

CONCLUSIONS

The aim set forth in the Introduction is to study the effectiveness of integral control in reducing trajectory errors caused by mass attraction. The findings and recommendations of this thesis are:

- Disturbing forces on the satellite which are fixed in the satellite frame of reference do not cause long term in-track trajectory errors. (Chapter III)

- The only external disturbing force on the satellite which will produce long term in-track trajectory error is the constant atmospheric drag. For typical satellites, specific drag force (f_{iD}) will be $10^{-2} > f_{iD} > 10^{-5}$ mm/sec^2 (Chapter III).

- Root locus and computer simulations of the integral controller showed that the system is unstable at high integral controller gain K_c. It also showed that there is always a range of stable K_c. (Chapter IV)

- Analysis of integral on-off controls with deadspace have shown that they can be analyzed with the root locus plots of a linear integral control. (Chapter IV)

- Taking all factors into consideration (stability, trapping susceptibility, etc.), for a satellite with deadspace size $r_d = 0.1$ mm, the following control parameter ranges are recommended: $K_p/\omega_s^2 > 1$, $3 > \gamma\omega_s > 1$, and $10^{-2} > K_c > 8 \times 10^{-4}$ 1/sec. (Chapter IV)

- In-track trajectory error (after 1 year) due to mass attraction was reduced from 150 km to 72 m with the use of integral control. This assumed an on-off controller with maximum force level of 0.01 mm/sec^2 and step sizes of 0.1 sec. (Chapter V)

- The maximum trajectory error due to limit cycle resonance, that can be expected in practice, is 1.5 km in the very unlikely event that it is allowed to limit cycle at frequency = 2/3 ω_h for 4 months (Chapter V).

- In a typical drag-free satellite, $5 \times 10^{-3} > \Delta V > 5 \times 10^{-4}$ mm/sec. The minimum $|\epsilon|$ for significant limit cycle frequencies is approximately 10^{-2} rad/sec. However, for $|\epsilon| > 10^{-5}$ rad/sec $|h|$ is already less than 2 percent of $|h|_{max}$, and it is inversely proportional to ϵ (for $|\epsilon| > 10^{-5}$ rad/sec). Therefore, trajectory

errors due to limit cycles will be negligible. ($j\omega_{LC} = 2\omega_h + \epsilon$) (Chapter V).

- Typically, in-track trajectory error of less than 0.9 km after 1 year will result from a spin rate mechanization error of less than 0.001 rad/sec. (Chapter V)

- For the recommended range of $K_p/\omega_s^2 > 1$, no significant gain in trapping susceptibility is possible through a change in K_p. However, circular deadspace is significantly less susceptible than square deadspace, in the range $K_p/\omega_s^2 > 1$. (Chapter (VI)

- For $K_p/\omega_s^2 < 1$, trapping susceptibility decreases very rapidly with the decrease of K_p/ω_s^2. (Chapter VI).

Appendix A

COMPUTER PROGRAM SIMULATING SATELLITE SYSTEM WITH ON-OFF, INTEGRAL CONTROL WITH OCTAGONAL DEADSPACE

1. Program simulates the satellite translational equations of motion [Eqs. (2.2a,b)], on-off integral control with octagonal deadspace. Program is in WATFIV language.

2. Input data: K_c, K_p, γ, r_d, f_{ix}, f_{iy}, f_{bx}, f_{by}, x_e, y_e, f_m, dV, ω_s, ω_o, $\bar{\omega}_h$, mass attraction gradients and initial conditions.

3. Output Data: x_b, y_b, x_{bi}, y_{bi}, f_{cx}, f_{cy}, f_{eh}, $\int_0^t f_{eh}\,dt$, h.

4. List of Symbols:

$$A(1) = \frac{\partial f_{ex}}{\partial x}$$

$$A(2) = \frac{\partial f_{ex}}{\partial y}$$

$$A(3) = \frac{\partial^2 f_{ex}}{\partial x^2}$$

$$A(4) = \frac{\partial^2 f_{ex}}{\partial y^2}$$

$$A(5) = \frac{\partial^2 f_{ex}}{\partial x \partial y}$$

$$A(6) = \frac{\partial^3 f_{ex}}{\partial x^3}$$

$$A(7) = \frac{\partial^3 f_{ex}}{\partial y^3}$$

$$A(8) = \frac{\partial^3 f_{ex}}{\partial x^2 \partial y}$$

$$A(9) = \frac{\partial^3 f_{ex}}{\partial x \partial y}$$

$$B(m) = \frac{\partial^i f_{ey}}{\partial x^j \partial y^k} \quad \text{(in same order as A(m)}$$

$$BX, BY = f_{bx},\ f_{by}$$

$$C = K_c$$

$$DV = dV$$

$$EX, EY = e_x,\ e_y$$

$$FEH = f_{eh}$$

$$FM = f_m$$

$$FXO, FYO = f_{xo},\ f_{yo}$$

$$IFEH = \int_0^t f_{eh}\, dt$$

$$P = K_p$$

$$R = \gamma$$

$$RD = r_d$$

$$XBI, YBI = x_{bi},\ y_{bi}$$

$$XE, YE = x_e,\ y_e$$

$$XU, YU = x_u,\ y_u$$

$X(1) = t$

$X(2) = x_b$

$X(3) = x_b'$

$X(4) = y_b$

$X(5) = y_b'$

$X(6) = I_{hc}$

$X(7) = I_{vc}$

$T = t$

$W = \omega_s$

$WO = \omega_o$

$WH = \omega_h$

$WHM = \overline{\omega}_h$

5. Listing of Programs:

C Main Program:

```
COMMON/NAME/W,WS,XE,YE,FI,BX,BY,EX,EY,WT,DV,FM
COMMON/NOME/R,C,XU,YU,RD,CS,SN,XBI,YBI,FX,FY,WH,WHT,WHM,WHMT
COMMON/NIME/Y(4),A(9),B(9),FEH,FEHI,FXO,FYO
COMMON/NEME/Z(7),DFEH2,WO,WOS
DIMENSION X(15)
EQUIVALENCE (X(1),T)
```

```
C     Constant parameters of the system are assigned values:

      DV=0.001
      FM=1.E-2
      RD=0.1
      R=20.
      W=0.1
      WS=W**2
      WO=.001
      WOS=WO**2
      WH=.099
      WHM=.099
      FI=1.E-4
      BX=0.0
      BY=0.0
      XE=0.0
      YE=0.0
      FXO=0.
      FYO=0.
      A(1)=1.E-10
      A(2)=1.E-10
      A(3)=1.E-11
      A(4)=1.E-11
      A(5)=1.E-11
      A(6)=1.E-12
      A(7)=1.E-12
      A(8)=1.E-12
      A(9)=1.E-12
      DO 2 I=1,9
    2 B(I)=A(I)

C     Values of  Kc  to be read in, and variables are initialized:

   10 READ,C
      IF(C.GT.10) GO TO 99
      DFEH2=0.
      WT=0.
      EX=0.
      EY=0.
      XBI=0.
      YBI=0.
      CS=0.
      SN=0.
      XU=0.0
      YU=0.0
      DO 4 I=1,4
    4 Z(I)=0.
      DO 3 I=1,4
    3 Y(I)=0.
      FEH = 0.
```

```
    FEHI=0.
    DO 1 I=1,15
  1 X(I)=0
```

C Output Commands:

```
    WRITE (6,15)
 15 FORMAT (1H150X4HDATA///,4X1HT,5X3HXBI,4X3HYBI,3X2HFX,3X2HFY,4X2HXB
   15X2HYB,6X3HFEH,8X4HIFEH,8X2HEH)
    DO 30 I=1,1500
    WRITE (6,20) X(1),XBI,YBI,FX,FY,X(2),X(4),FEH,FEHI,X(15)
 20 FORMAT (1X,F6.1,2F7.3,2F5.2,5E11.3)
 30 CALL RUK(X,DT,15)
    WRITE (6,20) X(1),XBI,YBI,FX,FY,X(2),X(4),FEH,FEHI,X(15)
    GO TO 10
 99 RETURN
    END
```

C Subroutine does numerical integration of differential equations given in subroutine DERIV:

```
    SUBROUTINE RUK(X,DT,N)
 RUNGE-KUTTA 4 TH ORDER
    COMMON/NOME/R,C,XU,YU,RD,CS,SN,XBI,YBI,FX,FY,WH,WHT,WHM,WHMT
    DIMENSION X(15),U(30),F(30),D(30)
    CALL PULSE(X,DT)
    CALL DERIV(X,D,DT)
    DO 101 I=1,N
101 U(I)=X(I)+0.5 *D(I)
    CALL DERIV(U,F,DT)
    DO 102 I=1,N
    D(I)=D(I)+2.0 *F(I)
102 U(I)=X(I)+0.5 * F(I)
    CALL DERIV(U,F,DT)
    DO 103 I=1,N
    D(I)=D(I)+2.0*F(I)
103 U(I)=X(I)+F(I)
    CALL DERIV(U,F,DT)
    DO 104 I=1,N
104 X(I)=X(I)+(D(I)+F(I))/6.0
    RETURN
    END
```

C Soubroutine simulates an on-off octagonal controller-mechanication of Fig. 13:

```
      SUBROUTINE PULSE(X,DT)
      COMMON/NAME/W,WS,XE,YE,FI,BX,BY,EX,EY,WT,DV,FM
      COMMON/NCME/R,C,XU,YU,RD,CS,SN,XBI,YBI,FX,FY,WH,WHT,WHM,WHMT
      COMMON/NYME/D(4),S(3),E,CN
      DIMENSION X(15)
      WT=W*X(1)
      WHT=WH*X(1)
      WHMT=WHM*X(1)
      DT=1.
      FX=0.0
      FY=0.0
      XU=-C*(X(6)*COS(WHMT)+X(7)*SIN(WHMT))
      YU=-C*(-X(6)*SIN(WHMT)+X(7)*COS(WHMT))
      EX=X(2)-XU+R*(X(3)-W*X(4))
      EY=X(4)-YU+R*(X(5)+W*X(2))
      E=0.414
      D(1)=E*EY-EX
      D(2)=EY-E*EX
      D(3)=EY+E*EX
      D(4)=E*EY+EX
      S(1)=0.7*(EX-EY)
      S(2)=0.7*(EX+EY)
      S(3)=0.7*(EY-EX)
      CALL SIGN(D(2),D(3),CN)
      IF (CN.LT.0.) GO TO 61
      CALL SIGN(D(1),D(2),CN)
      IF (CN.LT.0.) GO TO 62
      CALL SIGN(D(3),D(4),CN)
      IF (CN.LT.0.) GO TO 63
      CALL SIGN(D(1),D(4),CN)
      IF (CN.GT.0.) GO TO 64
      GO TO 70
   61 IF (EX.GT.RD) GO TO 71
      IF (EX.LT.-RD) GO TO 72
      GO TO 70
   62 IF (S(2).GT.RD) GO TO 73
      IF (S(2).LT.-RD) GO TO 74
      GO TO 70
   63 IF (S(1).GT.RD) GO TO 75
      IF (S(1).LT.-RD) GO TO 76
   65 IF (S(3).GT.RD) GO TO 77
      IF (S(3).LT.-RD) GO TO 78
      GO TO 70
   64 IF (EY.GT.RD) GO TO 77
      IF (EY.LT.-RD) GO TO 78
      GO TO 70
   71 FX=-FM
      GO TO 80
   72 FX=FM
      GO TO 80
```

```
73 FX=-FM
77 FY=-FM
   GO TO 80
74 FX=FM
78 FY=FM
   GO TO 80
75 FX=-FM
   GO TO 65
76 FX=FM
   GO TO 65
80 DT=DV/FM
70 RETURN
   END
```

```
      C     Subroutine checks the sign of AN and BN; if the signs are
      C     equal, then CN = +1., if the signs are opposite, then CN = -1.

   SUBROUTINE SIGN(AN,BN,CN)

 IF N=+1, SIGN(AN)=SIGN(BN)
 IF N=-1, SIGN(AN)#SIGN(BN)

   CN=-1.
   IF (AN.GT.0.) GO TO 51
   IF (BN.LT.0.) GO TO 52
   GO TO 53
51 IF (BN.GT.0.) GO TO 52
   GO TO 53
52 CN=1.
53 RETURN
   END
```

```
      C     Subroutine gives differential forms of:

      C     a.  equations of motion,

      C     b.  integral controller,

      C     c.  in-track mass attraction force, and

      C     d.  in-track trajectory error.
```

```
      SUBROUTINE DERIV(X,DX,DT)
      COMMON/NAME/W,WS,XE,YE,FI,BX,BY,FX,FY,WT,DV,FM
      COMMON/NOME/R,C,XU,YU,RD,CS,SN,XBI,YBI,FX,FY,WH,WHT,WHM,WHMT
      COMMON/NIME/Y(4),A(9),B(9),FEH,FEHI,FXO,FYO
      COMMON/NEME/Z(7),DFEH2,WO,WOS
      DIMENSION X(15), DX(15)
      WT=W*X(1)
      WHT=WH*X(1)
      WHMT=WHM*X(1)
      DX(1)=DT
      DX(2)=X(3) * DT
      Z(3)=WS*(X(2)-XE)+2*W*X(5)+FI*COS(WT)+FX+BX
      DX(3)=Z(3)*DT
      DX(4)=X(5)*DT
      Z(4)=WS*(X(4)-YE)-2*W*X(3)-FI*SIN(WT)+FY+BY
      DX(5)=Z(4)*DT
      DX(6)=(X(2)*COS(WHMT)-X(4)*SIN(WHMT))*DT
      DX(7)=(X(2)*SIN(WHMT)+X(4)*COS(WHMT))*DT
C
C     XB=X(2), YB=X(4)    FIND XBI, YBI
C
      CS=COS(WHT)
      SN=SIN(WHT)
      XBI = CS * X(2) - SN * X(4)
      YBI = SN * X(2) + CS * X(4)
C
C     FIND INTEGRAL EFFECT OF MASS ATTRACTION
C
      Y(1) = CS*FXO-SN*FYO
      DX(8) = Y(1)*DT
      Y(2) = (CS*A(1)-SN*B(1))*X(2)+(CS*A(2)-SN*B(2))*X(4)
      DX(9) = Y(2) * DT
      Y(3) = 0.5*((CS*A(3)-SN*B(3))*X(2)**2+(CS*A(4)-SN*B(4))*X(4)**2+(
     1(CS*A(5)-SN*B(5))*X(2))*X(4))
      DX(10) = Y(3) * DT
      Y(4) = 0.166*((CS*A(6)-SN*B(6))*X(2)**3+(CS*A(7)-SN*B(7))*X(4)**3
     1+((CS*A(8)-SN*B(8))*X(2)**2)*X(4)+((CS*A(9)-SN*B(9))*X(2))*X(4)**2
     2)
      DX(11) = Y(4) * DT
      FEH = Y(1) + Y(2) + Y(3) + Y(4)
      FEHI = X(8) + X(9) + X(10) + X(11)
```

```
C
C       FIND IN-TRACK TRAJECTORY ERROR DUE TO MASS ATTRACTION
C
        Z(1)=-CS*FXO+SN*FYO
        Z(2)=(-CS*A(1)+SN*B(1))*X(2)+(-SN*A(1)-CS*B(1))*(2*X(3))+(CS*A(1)-
       1SN*B(1))*Z(3)+(-CS*A(2)+SN*B(2))*X(4)+(-SN*A(2)-CS*B(2))*(2*X(5))+
       2(CS*A(2)-SN*B(2))*Z(4)
        Z(5)=(-CS*A(3)+SN*B(3))*X(2)**2+(-SN*A(3)-CS*B(3))*4*X(2)*X(3)
       1+(CS*A(3)-SN*B(3))*2*(X(2)*Z(3)+X(3)**2)
        Z(6)=(-CS*A(4)+SN*B(4)) *X(4)**2+(-SN*A(4)-CS*B(4))*4*X(4)*X(5)
       1+(CS*A(4)-SN*B(4))*2*(X(4)*Z(4)+X(5)**2)
        Z(7)=(-CS*A(5)-SN*B(5))*X(2)*X(4)+(-SN*A(5)-CS*B(5))*(X(2)*X(5)+
       1X(3)*X(4))*2+(CS*A(5)-SN*B(5))*(X(2)*Z(4)+X(3)*X(5)*2+Z(3)*X(4))
        DFEH2=Z(1)+Z(2)+0.5*(Z(5)+Z(6)+Z(7))
        DX(12)=(-WOS*X(13)+DFEH2-3*(WOS*FEH))*DT
        DX(13)=X(12)*DT
        DX(14)=X(13)*DT
        DX(15)=X(14)*DT
        RETURN
        END
$DATA
   0.004
   20.0
$STOP
/*
```

Appendix B

COMPUTER PROGRAM SIMULATING SATELLITE SYSTEM WITH ON-OFF, INTEGRAL CONTROL WITH SQUARE DEADSPACE

1. Delete subroutines PULSE and SIGN from program given in Appendix A.

2. Add new subroutine PULSE.

C Subroutine simulates an on-off square deadspace controller.

```
      SUBROUTINE PULSE(X,DT)
      COMMON/NAME/W,WS,XE,YE,FI,BX,BY,EX,EY,WT,DV,FM
      COMMON/NOME/R,C,XU,YU,RD,CS,SN,XBI,YBI,FX,FY,WH,WHT,WHM,WHMT
      DIMENSION X(15)
      WT=W*X(1)
      WHT=WH*X(1)
      WHMT=WHM*X(1)
      DT=1.
      FX=0.0
      FY=0.0
      XU=-C*(X(6)*COS(WHMT)+X(7)*SIN(WHMT))
      YU=-C*(-X(6)*SIN(WHMT)+X(7)*COS(WHMT))
      EX=X(2)-XU+R*(X(3)-W*X(4))
      EY=X(4)-YU+R*(X(5)+W*X(2))
      IF (EX.GT.RD) GO TO 50
      IF (EX.LT.-RD) GO TO 51
   60 IF (EY.GT.RD) GO TO 52
      IF (EY.LT.-RD) GO TO 53
      GO TO 70
   50 FX=-FM
      DT=DV/FM
      GO TO 60
   51 FX=FM
      DT=DV/FM
      GO TO 60
   52 FY=-FM
      DT=DV/FM
      GO TO 70
   53 FY=FM
      DT=DV/FM
   70 RETURN
      END
```

Appendix C

SCHEMATIC FOR ANALOG COMPUTER SIMULATION OF SATELLITE SYSTEM WITH SQUARE DEADSPACE, INTEGRAL, CONTROL

1. Simulation was done on EAI analog computer TR-48.
2. Schematic shows simulation of satellite translational equations of motion [Eq. (2.2a,b)], integral control with square deadspace.
3. Time scaled such that simulation time = 1/10 real time.
4. ω_s = 0.1 rad/sec.
5. Definition of symbols on next page.
6. Figures 25 and 26 show the schematics for analog computer simulation of the satellite system with linear square deadspace; integral control.

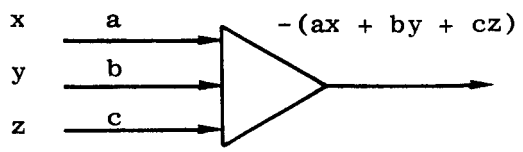

operational amplifier

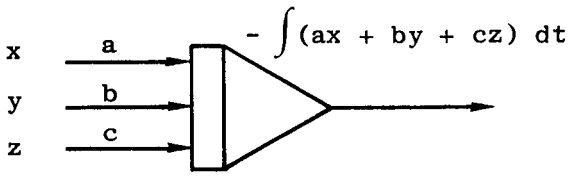

integrator

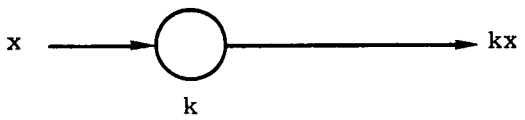

potentiometer (2 sided)

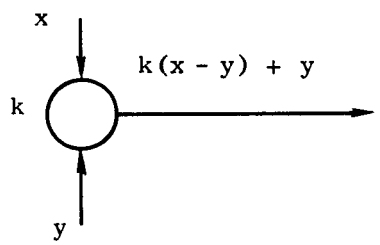

potentiometer (3 sided)

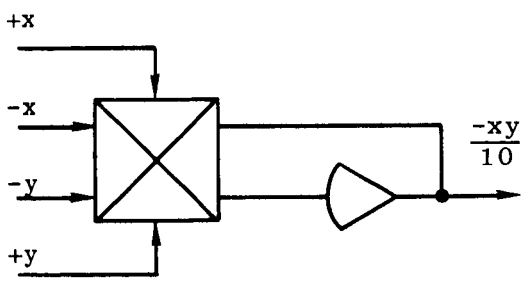

multiplier

diode

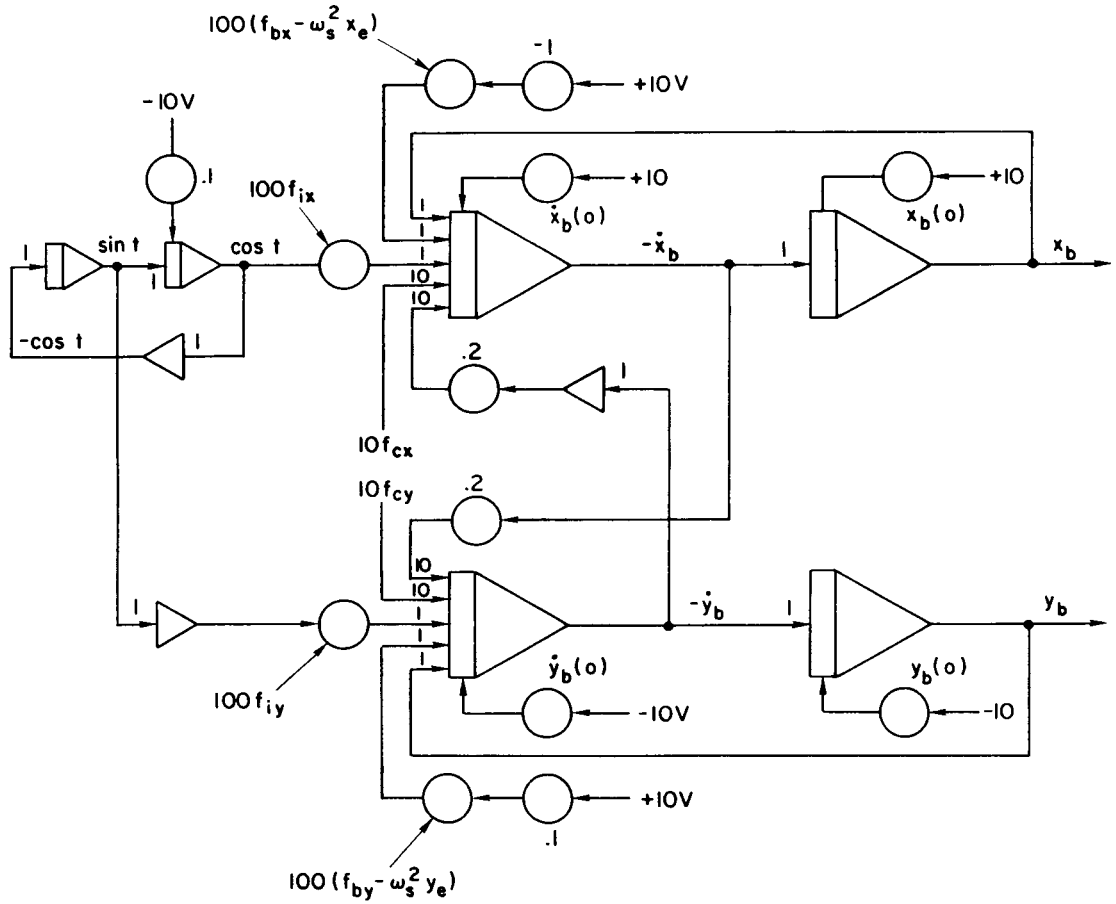

Fig. 25. ANALOG SIMULATION OF TRANSLATIONAL EQUATIONS OF MOTION [Eq. (2.2a,b)].

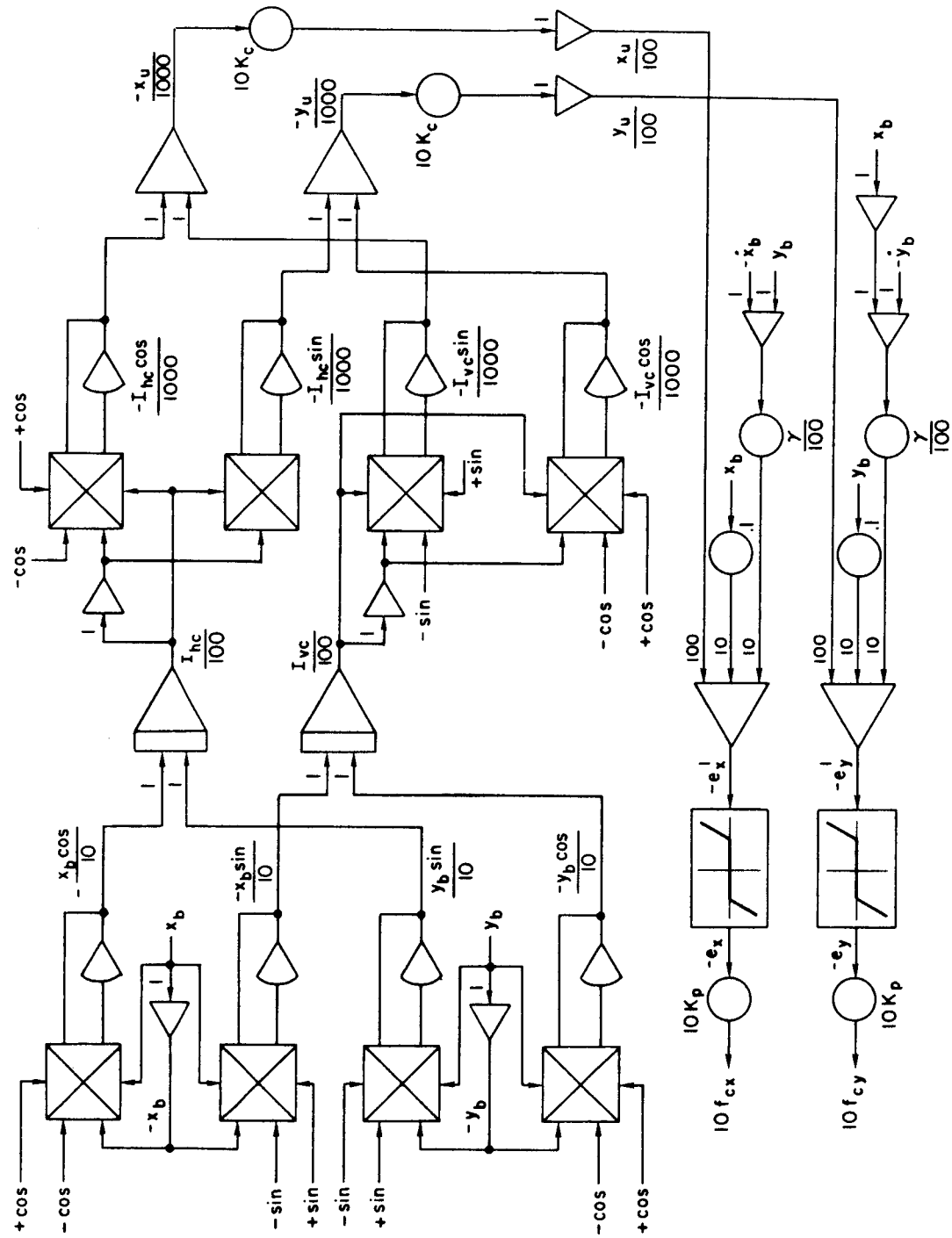

Fig. 26a. ANALOG SIMULATION OF INTEGRAL CONTROLLER WITH SQUARE DEADSPACE.

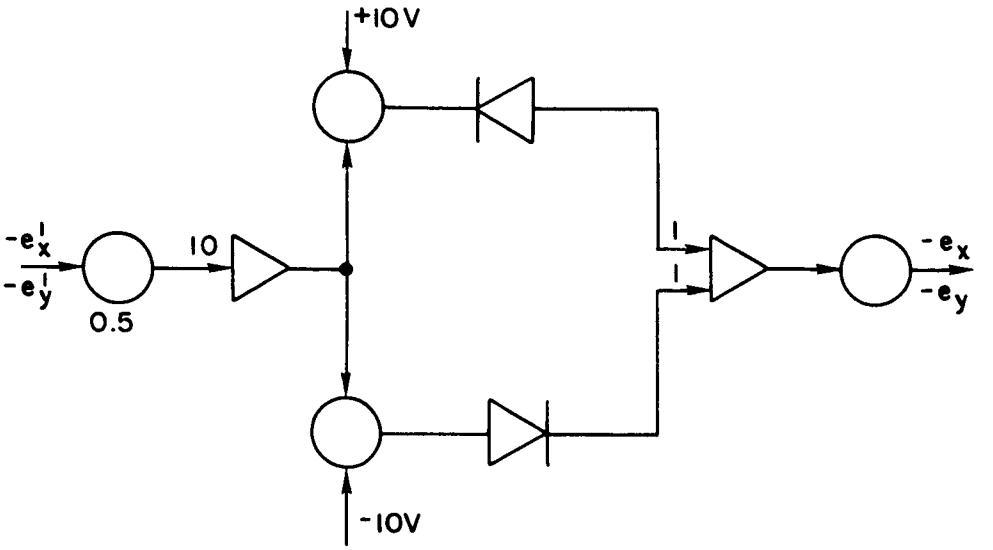

Fig. 26b. SCHEMATIC OF SQUARE DEADSPACE.

REFERENCES

1. J. D. Powell and B. O. Lange, "Control of a Spinning Drag-Free Satellite with an Application of Estimation Theory," SUDAAR Rept. No. 402, Stanford University, Stanford, Calif., May 1970.

2. B. Lange, "The Control and Use of Drag-Free Satellite," SUDAER Rept. No. 194, Stanford University, Stanford, Calif., Jun 1964.

3. A. W. Fleming, "Mass Attraction Properties of Drag-Free Satellites," to be published.